UNIVERSITY OF TURKU

Growth characteristics and antibody detection of human parechovirus types 1-6 in the intestinal HuTu80 cell line

Master's thesis
Master's degree in biomedical imaging
40 ECTS
Faculty of Medicine
University of Turku

Omorovbiye Omorevbarhia

10.05.2026

Supervisor:
Petri Susi (Ph.D.)
Institute of Biomedicine
University of Turku

Master's thesis

Subject: Master's degree in biomedical imaging

Author(s): Omorovbiye Omorevbarhia

Title: Growth characteristics and antibody detection of human parechovirus types 1-6 in the intestinal HuTu80 cell line.

Supervisor(s): Petri Susi (Ph.D.)

Number of pages: 71 pages

Date: 12.05.2026

Abstract

Human parechoviruses (PeVs) are common pathogens associated with a wide clinical spectrum ranging from mild respiratory and gastrointestinal symptoms to severe, life-threatening neurological infections, particularly in infants. While nucleic acid detection methods such as PCR are considered the diagnostic gold standard due to their high sensitivity and specificity, their cost limits diverse use in resource-limited settings. Viral culture remains a more accessible alternative; however, its application is limited by the absence of a universal cell line capable of supporting the replication of multiple PeV-A genotypes. This study aimed to evaluate the permissiveness of the HuTu80 cell line for the replication of PeV-A genotypes and to identify suitable antibodies for viral detection. The in vitro growth characteristics of PeV-A1 to PeV-A6 strains in HuTu80 cells were assessed using cytopathic effect (CPE) analysis, immunofluorescence assay (IFA), real-time RT-qPCR, and ELISA. The most suitable antibody was subsequently used to compare viral replication in HuTu80, HT-29, and Vero E6 cell lines. The results demonstrated that all six PeV-A genotypes replicated efficiently in HuTu80 cells, with time- and strain-dependent cytopathic effects observed within 24 hours post-infection. Both the monoclonal antibody P5C4 and several polyclonal antibodies (K8873, K8851, K306, and K316) successfully detected all six genotypes; however, P5C4 was selected for further analyses due to its specific recognition of the PeV-A1 VP0 protein. Comparative analyses showed that HuTu80 and HT-29 cells were permissive to PeV-A infection and compatible with immunofluorescence-based detection of viral antigens, whereas Vero E6 cells were not suitable for this application. Overall, these findings demonstrate that HuTu80 cells represent a useful additional cell line for the cultivation, isolation, and antibody-based visualization of PeV-A, and that specific antibodies, particularly P5C4, provide effective tools for detecting parechoviruses. Together, these may help improve laboratory strategies for molecular analysis of parechoviruses and their detection.

Keywords: Parechovirus, Replication, HuTu80 cell, RT-qPCR, CPE, Antibodies, IFA, and ELISA.

List of abbreviations

ATCC	American Type Culture Collection
BCA:	Bicinchoninic acid.
BSA:	Bovine serum albumin.
BM:	Biomolecular systems.
cDNA:	Complementary DNA
CIM:	Convective interaction media
CNS:	Central nervous system
CPE:	Cytopathic effect.
Ct:	Cycle threshold
DAPI:	4′,6-diamidino-2-phenylindole
DMEB:	Dulbecco's modified Eagle medium
DNA:	Deoxyribonucleic acid
DPI:	Day-post-infection
dsRNA:	Double-stranded ribonucleic acid
ELISA:	Enzyme-linked immunosorbent assay
EMEM:	Eagle’s minimum essential medium
ER:	Endoplasmic Reticulum
FCS:	Fetal calf serum
FBS:	Fetal bovine serum
FPLC:	Fast protein liquid chromatography
GIT	Gastrointestinal Intestinal tract
GST:	Glutathione S-transferase
HAE:	Human airway epithelial
HRP:	Horseradish peroxidase
HT29:	Human colon adenocarcinoma cell lines
HuTu80:	Human duodenum adenocarcinoma cell lines
IFA:	Immunofluorescence assay
IVT-RNA:	In vitro transcribed-RNA
Mab:	Monoclonal antibody
MIC:	Magnetic Induction Cycler
MOI:	Multiplicity of infection
MYADM:	Myeloid-associated differentiation marker

NTC:	No template control
NT:	Nucleotide
ORF:	Open reading frame
PAb:	polyclonal antibody
PBS:	Phosphate-buffered saline
PBS-T:	Phosphate-buffered saline with Tween 20
PCR:	Polymerase chain reaction
PeV:	Parechovirus
PeV-A:	Parechovirus ahumpari
PFA:	Paraformaldehyde
RGD:	Arginine-glycine-aspartic acid
RNA:	Ribonucleic acid
RT-qPCR:	Reverse transcription quantitative polymerase chain reaction
SARS-CoV-2:	Severe acute respiratory syndrome coronavirus 2
r-Protein G:	recombinant protein G
TBS:	Tris-buffered saline
TBST:	Tris-buffered saline with Tween-20
scFv:	Single chain variable fragment
UTR:	Untranslated region
VP:	Viral protein
VP0:	Viral protein 0
VPI:	Viral protein 1

Table of contents

1. Literature overview

1.1 Introduction

Viruses continue to place a steady strain on global health, whether they emerge suddenly as new threats or persist quietly as long-standing infections. While not a pandemic threat like SARS-CoV-2, parechovirus (PeV) is a significant and potentially severe pathogen for a specific, vulnerable demographic: infants and young children, representing a leading causative factor of neonate diseases such as viral meningitis and sepsis-like illness (Harvala et al., 2011). Parechoviruses belong to the *Picornaviridae* family, which consists of a large group of small non-enveloped viruses with a monopartite, single-stranded, positive-sense RNA genome (Alam et al., 2025). In addition to humans, parechovirus-like viruses have been found in many vertebrate and invertebrate species. These viruses are very adaptable from an evolutionary view because of their ability to infect a wide range of vertebrate and invertebrate species (Andino et al., 2023).

While most parechoviral infections are asymptomatic, some infected newborns and infants develop serious neurological symptoms (Harvala et al., 2010). Parechoviruses utilize a dual transmission strategy, faecal-oral and respiratory mode, which means they can thrive and replicate in the human GIT and respiratory tracts (Esposito et al., 2014; Wang et al., 2020). This route of transmission reflects the virus's enteric tropism, which accounts for its efficient spread in community settings, particularly among infants and young children in daycare or household environments where maintaining hygiene practices can be challenging. This enteric tropism is very relevant for studies using intestinal epithelial cell lines such as HuTu80, which model the natural site of early viral replication.

1.2 Classification within the *Picornaviridae* family

The order *Picornaviridae* comprises 40 genera, and these viral categories majorly infect vertebrates, with their initial classification historically based upon primary infection sites and antigenic relationships (Andino et al., 2023). Meanwhile, since immune-competent animal models are lacking for most picornaviruses, this caused a shift in classification toward methods based on laboratory neutralization tests and genetic analysis of viral RNA and protein sequences (Zell et al., 2021). Recent Picornavirus classification is mainly based on the similarities in the amino acid sequences of structural proteins and the non-structural proteins 2C, 3C, and RNA-

dependent RNA polymerase, especially because of the development of many new viruses (King et al., 2018).

According to recent studies, of the classification of *Picornaviridae* genera, eight of them contain human pathogens (Joki-Korpela & Hyypiä, 2001). *Parechovirus* genus comprises six major species (A-F), of which include *Parechovirus ahumpari* (PeV-A), which contains human-infecting viruses (Stanway et al., 1994).

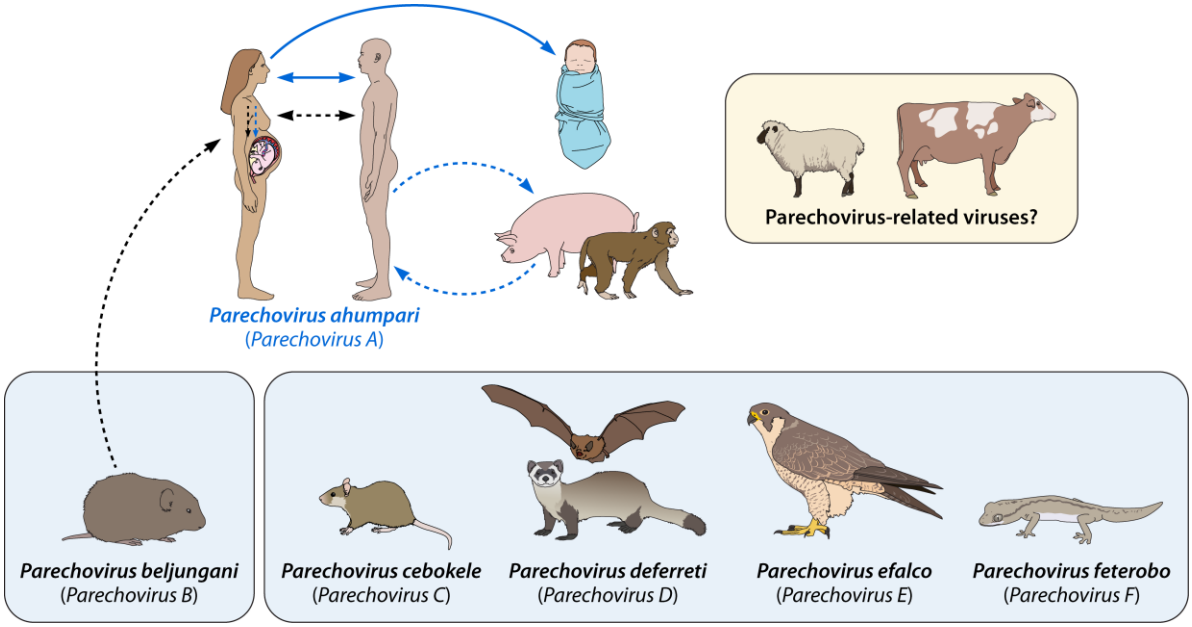

Figure 1: Host range and transmission of parechoviruses. Parechovirus genotypes and their sources (Alam et al., 2025). This image was reprinted with the permission of the copyright holder under the license: https://creativecommons.org/licenses/by/4.0/.

1.3 Human parechovirus (PeV-A) genotypes

The widespread use of genome sequencing between 2004 and 2019 led to the identification of 16 new PeV-A genotypes based on differences in the VP1 sequence. Strains of *Parechovirus A* species (PeV-A) differ widely in the hosts they can infect, the viral proteins they use, and how they exploit host cell lipids and proteins at different stages of their life cycle (Alam et al., 2025). According to Alam et al. (2025), the first PeV-A strains were identified in the United States (A1, A2, and A5), followed by Japan (A3 and A6), the Netherlands (A4 and A14), Pakistan (A7), Brazil (A8), Bolivia (A9–A13 and A15–A16), Ivory Coast (A17), Ghana (A18), and Malawi (A19).

Among the 19 recognized *Parechovirus A* genotypes, types 1–6 (PeV A1 to PeV A6) are the most commonly detected in human clinical samples (Benschop et al., 2008). Although these genotypes are genetically related, they differ in their epidemiology, receptor usage, cytopathic

effect (CPE), growth behaviour, and diagnostic detectability (Merilahti et al., 2016; Westerhuis et al., 2013). These differences are important to understand because they influence how the viruses behave in cell culture and how reliably they can be identified using serological or molecular methods (Renaud et al., 2011; Tripathi et al., 2021a).

1.3.1 Parechovirus type 1 (PeV-A1)

The prototype strains for PeV-A1 (Harris) were first identified and obtained from paediatric faecal samples in 1956 by Albert Sabin and Reinhard Wigand (Wigand & Sabin, 1961). Parechovirus-A1 is the most frequently detected human parechovirus worldwide and is the main genotype associated with mild gastrointestinal and respiratory disease in early childhood. The ubiquity of PeV-A1 reflects its efficient transmission and strong enteric tropism, as seen by its consistent detection in stool samples across multiple epidemiological studies (Benschop et al., 2010; Ito et al., 2010). From a virological standpoint, PeV A1 is one of the easiest parechoviruses to cultivate. It replicates efficiently in several cell lines, including HT29, Vero, and LLC-MK2, producing a clear cytopathic effect (CPE) characterized by cell rounding, shrinkage, and detachment (Westerhuis et al., 2013). This reliable CPE has historically made PeV-A1, Harris, the reference strain for laboratory studies.

PeV-A1 utilizes αVβ1 integrin as a primary entry receptor (Merilahti et al., 2016). Recent work has identified MYADM as an essential host protein facilitating viral entry (Qiao et al., 2024). These findings show a receptor pattern different from many enteroviruses and help explain the strong affinity of PeV-A1 for intestinal epithelial cells (Qiao et al., 2024). Diagnostic detection of PeV-A1 in clinical samples has been established in previous studies. Molecular assays, such as PCR-based tests, reliably identify the virus in stool and respiratory samples (Benschop et al., 2008; Westerhuis et al., 2013). Also, serological detection has been enhanced by VP0-based synthetic peptide assays (Abed et al., 2007). Because of these reliable diagnostic tools and the strong ability of PeV-A1 to grow in cell culture, PeV-A1 remains the most extensively studied and best-characterized genotype among the PeV A1-A6 group (Benschop et al., 2010; Westerhuis et al., 2013).

1.3.2 Parechovirus type 2 (PeV-A2)

Based on the parechovirus taxonomy, the PeV-A2 stays in a distinct position in the classification. Previously classified as Echovirus 23, it was subsequently reclassified following molecular analyses revealing key differences from enteroviruses and clear similarities with the

parechovirus genus (Ghazi et al., 1998; Stanway et al., 1994). The earlier misclassification of PeV-A2 highlights how unique it is antigenically from other parechoviruses (Ghazi et al., 1998; Stanway et al., 1994). When compared with PeV-A1, PeV-A2 shows more variable growth characteristics in vitro; it can replicate in standard enteric cell lines but typically does so more slowly and with a weaker cytopathic effect. Its intracellular replication complexes resemble those of PeV-A1 (Krogerus et al., 2003), yet its antigenic differences influence neutralization patterns and likely contribute to its limited detection in serological studies (Ghazi et al., 1998).

Based on clinical experiments, PeV-A2 is detected less frequently than PeV-A1, and its disease associations remain poorly defined due to limited surveillance data (Benschop et al., 2008). Although PCR-based detection is reliable, serological assays built around PeV-A1 antigens often fail to capture PeV-A2 exposure because of its antigenic divergence (Ghazi et al., 1998; Stanway et al., 1994). Thus, PeV-A2 is still relatively understudied, and several aspects of its epidemiology and pathogenic potential remain unclear (Benschop et al., 2008).

1.3.3 Parechovirus type 3 (PeV-A3)

Another class, PeV-A3, is commonly known as the most clinically significant parechovirus genotype, because it is strongly linked to severe neonatal illness, including sepsis-like presentations, meningitis, and white-matter injury (Harvala et al., 2011; Verboon-Maciolek et al., 2008). PeV-A3 was earlier identified from a case of transient paralysis in 1999 and reported in 2004 (Al-Sunaidi et al., 2007). Unlike PeV-A1, infections caused by PeV-A3 often show very high viral loads but relatively little or no inflammation, which makes the illness harder to recognise clinically and can delay diagnosis (Harvala et al., 2010). Also, PeV-A3 is one of the most difficult genotypes to cultivate. It tends to grow poorly in many standard cell lines and often shows weak or delayed cytopathic effects (CPE) (Westerhuis et al., 2013). This limited growth has made it harder to study PeV-A3, in some cases, contributing to delays in detection.

An important step in understanding PeV-A3 biology was the identification of MYADM as a key factor required for host-viral entry (Watanabe et al., 2023). In contrast to PeV-A1, PeV-A3 does not efficiently use αVβ1, αVβ3, or αVβ6 integrins (Seitsonen et al., 2010), suggesting that it relies on a different entry mechanism. This difference may help explain why PeV-A3 has more restricted cell tropism and distinct clinical features.

PeV-A3 is also the most detected parechovirus in cerebrospinal fluid (Harvala et al., 2011). While molecular detection methods are reliable, serological assays remain challenging due to

limited cross-neutralization between PeV-A types (Westerhuis et al., 2013). Hence, the association of PeV-A3 with more severe disease, along with its restricted growth and distinct receptor usage, makes PeV-A3 an important focus in parechovirus studies.

1.3.4 Parechovirus type 4 (PeV-A4)

PeV-A4 is reported less often than PeV-A1 or PeV-A3, but it is still an important circulating genotype, especially in children. It is frequently detected in stool samples from paediatric patients with gastroenteritis (Alam et al., 2013), which describes its enteric nature. In vitro studies have reported that PeV-A4 shows moderate growth and replicates in several cell lines, producing cytopathic effects (CPE) that are generally weaker than those of PeV-A1 but more consistent than those observed with PeV-A3 (Westerhuis et al., 2013). However, PeV-A4 has not been studied extensively, and there is still limited information on its receptor usage and antigenic properties.

Diagnostic detection of PeV-A4 relies mainly on molecular assays, since serological tools for this genotype are still limited (Westerhuis et al., 2013). Its detection in pediatric cases suggests that PeV-A4 contributes to the overall challenges of enteric infections, although its clinical severity is generally lower than that associated with PeV-A3 (Benschop et al., 2008).

1.3.5 Parechovirus type 5 (PeV-A5)

PeV-A5 is one of the less well-characterized parechovirus genotypes. It is detected only occasionally in stool samples and is mainly associated with gastrointestinal symptoms, with some reports of mild respiratory illness (Al-Sunaidi et al., 2007; Baumgarte et al., 2008). Al-Sunaidi et al. (2007) also reported that this genotype was first isolated in 1986 from a febrile child in Connecticut and was reclassified as PeV-A5 in 2007. The circulation of PeV-A5 appears to vary between regions, with some areas reporting higher prevalence than others. In cell culture, PeV-A5 shows varying replication. It can grow in several commonly used cell lines, but often produces weak or subtle cytopathic effects (CPE), which can make visual detection more difficult (Baumgarte et al., 2008). This low-CPE phenotype may partly explain why it is not always easily identified in laboratories that rely on culture-based methods.

Additionally, PeV-A5 shows limited cross-neutralization with other genotypes, suggesting the need for more specific serological tools (Al-Sunaidi et al., 2007). The development of VP0-

targeting monoclonal antibodies that can recognize multiple genotypes, including PeV-A5, offers a useful approach to improve detection (Tripathi et al., 2021a).

1.3.6 Parechovirus type 6 (PeV-A6)

PeV-A6 is closely related to PeV-A4 and PeV-A5 and is mainly detected in stool samples from children with gastroenteritis (Alam et al., 2025; Alam et al., 2013). Although it is reported less often than PeV-A1 or PeV-A3, it adds to the diversity of circulating parechoviruses. While PeV-A6 shows variable replication in vitro, they are slightly similar to PeV-A5. They often produce mild or delayed cytopathic effects (CPE), which can make it harder to identify based on cell culture alone (Westerhuis et al., 2013). This emphasizes the reasons why molecular methods are important for reliable detection.

Based on serological studies, PeV-A6 is difficult to distinguish from closely related genotypes due to limited cross-neutralization (Al-Sunaidi et al., 2007; Drexler et al., 2009). Monoclonal antibodies targeting VP0 with broader reactivity may help to improve PeV-A6 detection (Tripathi et al., 2021a), although more work is still needed to better understand its antigenic properties.

1.4 Human parechovirus (PeV-A): structure and viral proteins

Structurally, parechoviruses are small virions with a diameter of 28 nm, non-enveloped viruses that carry a positive-sense RNA genome within a smooth, proteinaceous capsid (Schnurr et al., 1996). The virus particles of PeV-A are enclosed by an icosahedral capsid, which is formed by structural proteins encoded alongside the non-structural proteins required for viral replication. Parechoviral genomes are 7,300–7,600 nucleotides long, consisting of a single open reading frame flanked by untranslated regions (UTRs), with the 5' UTR covalently linked to the viral protein, VPg, via a tyrosine residue (Shakeel et al., 2016). Basically, the PeV-A genome is divided into four different areas: the 5' untranslated region (UTR), one open reading frame (ORF), the 3' UTR, and a poly(A) tract.

The 5' UTR is folded into long hairpin structures containing a type II internal ribosome entry site (IRES), enabling cap-independent translation of the viral polyprotein, which is subsequently cleaved into the mature precursors P1, P2, and P3 (Stanway & Hyypiä, 1999). Initial characterization of these viruses revealed unique growth properties, including a

cytopathic effect primarily at the periphery of the cell sheet and distinctive nuclear changes, such as the disappearance of the nucleus and chromatin (Shaver et al., 1958).

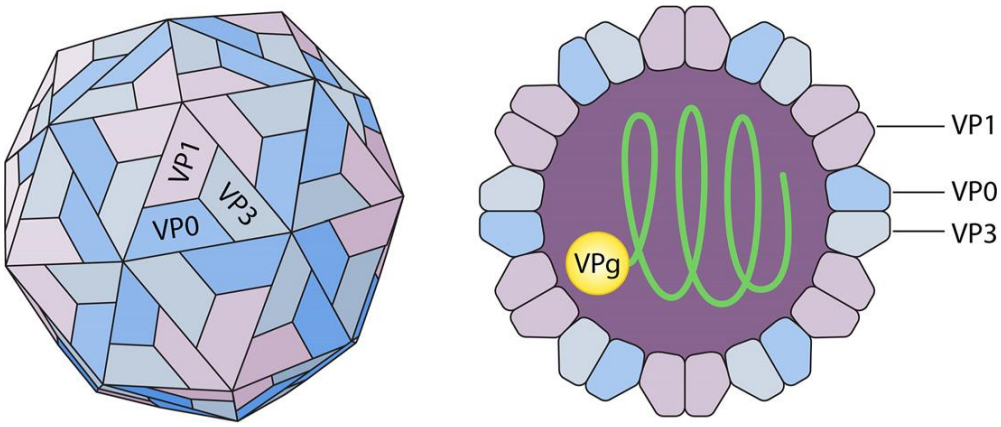

Figure 2: Parechovirus A species genome structure (Walls, 2017)**.** This image describes the structural viral proteins present in the PeV-A genome. The image was reprinted with the permission of the copyright holder under the license: https://creativecommons.org/licenses/by/4.0/.

The P1 region of human parechoviruses encodes the capsid precursor polyprotein. After post-translational cleavage, this polyprotein typically yields the three structural proteins VP0 (1AB), VP3 (1C), and VP1 (1D), as in Figure 2 (Alam et al., 2025). Parechoviruses display distinctive molecular features relative to other members of the *Picornaviridae* family, characterized by the absence of VP0 cleavage into VP2 and VP4 during capsid maturation, as well as divergences in the structure and function of their non-structural proteins (Ghazi et al., 1998; Stanway et al., 1994).

Structural analyses indicate that the uncleaved N-terminus of the VP0 protein, which corresponds to the VP4 domain, plays a critical role in stabilizing the inner surface of the icosahedral capsid, possibly through interactions with the viral RNA genome or other capsid subunits (Shakeel et al., 2016). Meanwhile, from Figure 3, the P2 and P3 polyprotein regions are processed into seven non-structural proteins (2A, 2B, 2C, and 3A, 3B, 3C, 3D). These proteins are essential for viral replication and pathogenesis, playing crucial roles in RNA replication, host cell membrane remodelling, and immune evasion (Alam et al., 2025).

Studies have demonstrated that VP1, the predominant capsid protein and primary carrier of B-cell antigenic epitopes in picornaviruses (e.g., polioviruses), constitutes the principal target of virus-neutralizing antibodies (Minor et al., 1986). In PeV-A1, a linear epitope is located within VP1, while residues contributing to two conformational epitopes are distributed across multiple capsid proteins. Immunological mapping using rabbit antibodies and synthetic peptides has

further identified an additional immunogenic region within VP0 and another one at the C-terminus of VP1 (Joki-Korpela et al., 2000).

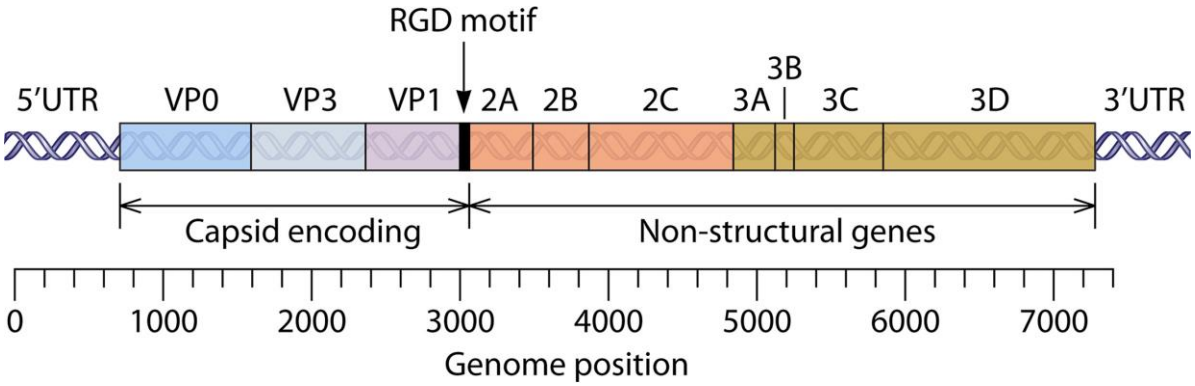

Figure 3: Human parechovirus virion genome organization (Harvala et al., 2010; Walls, 2017). This image explains all the structural proteins and non-structural translated proteins in the PeV-A genome. The image was reprinted with the permission of the copyright holder under the license: https://creativecommons.org/licenses/by/4.0/.

1.5 PeV-A entry and host recognition

Mostly, viral entry of PeV-A genotypes encodes the integrin-binding RGD (arginine-glycine-aspartic acid) motif in the VP1 capsid protein. RGD is primarily used in interactions with host cell integrins α5β1, αvβ3, and αvβ6, which thus function as attachment and entry receptors for parechoviruses in Figure 4 (Merilahti et al., 2016; Seitsonen et al., 2010). Additionally, heparan sulfate and β2-microglobulin have been implicated in facilitating PeV-A attachment to specific host cells. These studies suggest that this RGD motif seems to be essential for the infectivity of PeV-A1,-2, -4, and -5, but PeV-A3 differs from these genotypes because it lacks the RGD motif, suggesting that it utilizes an alternative receptor and a distinct mechanism for host cell entry (Al-Sunaidi et al., 2007).

Recent studies show that MYADM may function as a cellular receptor for PeV-A3 and possibly also as an alternate receptor for PeV-A1 and A2 (Qiao et al., 2024; Watanabe et al., 2023). This change in receptor usage (interaction with the fourth extracellular loop of MYADM) may shift tissue tropism, possibly contributing to the distinct epidemiology and clinical presentation of PeV-A3 infections compared to other genotypes (Benschop et al., 2008). Moreover, several strains of PeV-A1, -5, -7, -8, -10, -11, -13, -14, and -15 have been reported to lack the RGD motif (Alam et al., 2013; Qiao et al., 2024). This basically implies that parechoviruses may use different receptors in different cell lines or may need many receptors for cell entry.

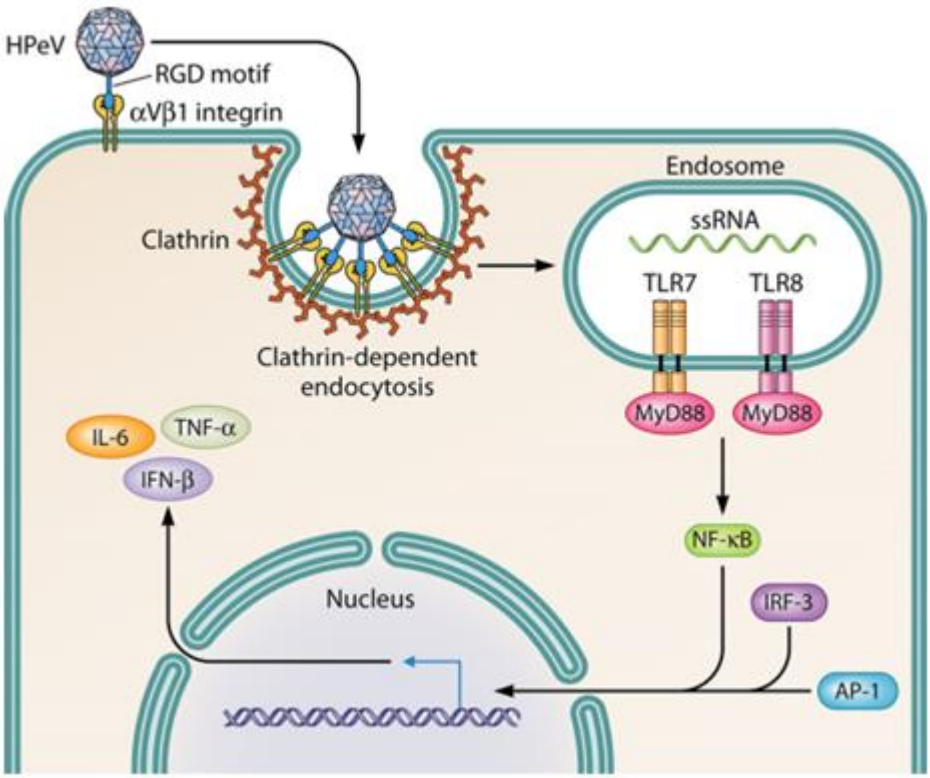

Figure 4: PeV-A cell entry (Walls, 2017). PeV-A initiates cell entry when the RGD motif in its capsid attaches to αVβ1 integrin on the host cell surface. This interaction triggers clathrin-mediated endocytosis, resulting in viral internalization into endosomes. Within the endosome, this entry process initiates a downstream signaling cascade. This image was reprinted with the permission of the copyright holder under the license: https://creativecommons.org/licenses/by/4.0/.

1.6 Cell cycle and viral replication

Even though there is limited experimental evidence of PeV-A protein translation and viral genome replication, most host ribosomes primarily translate positive-sense viral RNA into a polyprotein precursor (Alam et al., 2025). Once PeV-A has attached itself to its cellular receptor, the viral capsid is brought into the host cell by the endocytic pathway, quickly followed by genome release into the cytoplasm, the site of viral replication (Andino et al., 2023). After PeV-A virion entry into the cytoplasm, the positive-stranded viral RNA is translated to produce viral proteins, including the viral RNA-dependent RNA polymerase needed for genome replication, RNA synthesis, and capsid formation. Once sufficient capsid proteins are ready, the P1 precursor is cleaved and assembled into pentamers, which then associate with newly synthesized positive-stranded RNA to form infectious virus particles (Andino et al., 2023).

Studies have shown that PeV-A1 proteins are detectable in the cellular endoplasmic reticulum (ER) within 30 minutes post-infection and subsequently localize to the cis-Golgi network at 60 minutes, and that capsid polypeptides are synthesized and can be observed in the cytoplasm by 4 hours post-infection, resulting in the completion of a full replication cycle within 6 to 8 hours (Joki-Korpela et al., 2001). After staining viral RNA with bromodeoxyuridine, post-infection changes in infected cells include a dilated ER, with little or no ribosomes, and a completely dispersed Golgi complex containing trans-Golgi marker, 1,4-galactosyltransferase, and non-structural protein 2C (Alam et al., 2025; Krogerus et al., 2003).

1.7 Clinical Manifestation and Pathogenesis of Parechoviruses

Human PeV primarily targets the gastrointestinal and respiratory tracts, which are likely the primary sites of viral replication. In some cases, the virus can disseminate via the bloodstream, leading to systemic infection and involvement of secondary replication sites such as the brain and liver (Harvala et al., 2010). Transmission of the PeV-A occurs primarily among children under 2 years old, and the risk of severe PeV-A3 infection is higher in families with siblings younger than 2 years (Wang et al., 2020). The transmission occurs primarily via the fecal–oral route from both asymptomatic and symptomatic individuals, with prolonged stool shedding between 2–24 weeks, while respiratory transmission appears less common but may contribute to infection in children with CNS involvement and is associated with a shorter shedding period of approximately 1–3 weeks (Wildenbeest et al., 2016).

While most parechoviral infections are asymptomatic, clinical symptoms range from mild cold-like illnesses, fever, stomach upset (nausea, vomiting, diarrhea), rash, encephalitis, pneumonia, loss of appetite in infants, to severe brain and nervous system infections and flaccid paralysis (Padala & Kallam, 2025; Verboon-Maciolek et al., 2008; Walls, 2017). The human PeV (PeV-A3) is identified as the second leading cause of viral sepsis-like illness and meningitis in neonates and infants (Wolthers et al., 2008). Although PeV-A is most often found in children, infections have also been reported in immunocompromised adults (Alshammari et al., 2024; Brouwer et al., 2020). According to studies, PeV-A infection of the central nervous system (CNS) can disrupt normal neuro-development in infants, resulting in long-term consequences such as speech impairment, motor abnormalities, visual impairment, and/or cerebral palsy (Britton et al., 2018).

1.8 Diagnosis and treatment of PeV-A

Because the clinical manifestations of PeV infections are diverse and often resemble those caused by other pathogens, laboratory testing is essential for accurate diagnosis. For many years, viral culture served as the primary method for diagnosing PeV-A infections, after which virus neutralization assays were used to determine the specific type (Benschop et al., 2010; Ito et al., 2010). But the commercial reagents required for this method are presently restricted to a few PeV-A types, mostly the PeV-A1 and PeV-A2 (Walls, 2017). Currently, reverse transcription quantitative polymerase chain reaction (RT-qPCR) serves as the primary method for laboratory confirmation of PeV-A (Renaud et al., 2011). Although PCR methods are highly specific and sensitive, they are expensive and not readily available in developing nations (Tripathi et al., 2021a).

Although the antigenic diversity of PeV capsids has prevented the development of broadly specific antibodies, recent serological evidence suggests that conserved regions within parechoviral capsids exist, which could serve as functional immunogenic targets for developing specific monoclonal antibodies (Abed et al., 2007). This has prompted the development of monoclonal antibodies targeting the PeV-A1 VP0 protein for the diagnosis of a broad range of parechovirus infections. As a result, since there are no antivirals or vaccines available to combat PeV-A infection, it has become paramount to identify a universal or standard cell line suitable for cultivating PeV-As for molecular analyses.

1.9 Parechoviral antibodies and serological detection of parechoviruses in relation to antibody-based assays

Antibodies are central in the interpretation of parechoviral infection patterns, estimation of population immunity, and assessment of the detection of different genotypes in both clinical and experimental settings. For PeV types 1–6, serological methods have developed more slowly than molecular diagnostics. This may be due to the broad antigenic differences between genotypes and the limited availability of genotype-specific reagents such as parechoviral antibodies. The high antigenic differences of PeV capsids likely explain the absence of reactive antibodies for their detection. Consequently, no specific antibodies are currently available for identifying these viruses.

Early-phase serological assays were largely based on PeV-A1 antigens, which limited their ability to detect antibodies against more distinct types, such as PeV-A2, A4, A5, and A6. These

studies have shown that parechovirus capsid proteins, particularly VP0 and VP1, vary between genotypes, leading to limited cross-neutralization (Al-Sunaidi et al., 2007; Joki-Korpela et al., 2000). Because of this, infections caused by non-PeV-A1 genotypes may have been underreported in serological studies, even when molecular methods confirm their presence.

To improve detection, some studies have explored peptide-based assays targeting conserved regions of VP0. For example, synthetic VP0-derived peptides have been used to detect antibodies across multiple genotypes, providing a more consistent alternative to whole-virus antigen formulations (Abed et al., 2007). However, these approaches may still show lower sensitivity for more antigenically distinct genotypes such as PeV-A5 and A6, highlighting the need for better tools that can cover a wider range of parechoviruses (Al-Sunaidi et al., 2007; Drexler et al., 2009).

More recent studies suggest that monoclonal antibodies targeting conserved VP0 regions have shown potential for broader parechoviral detection. These antibodies can recognize several PeV genotypes, including types 1 to 6, and may help improve the consistency of serological assays (Tripathi et al., 2021). Despite these improvements, there is no universal antibody that can detect most PeV types 1 to 6, and/or distinguishing between genotypes based on antibody responses remains difficult. Studies on PeV-A4, A5, and A6 have shown limited antigenic overlap, resulting in difficult differentiation of these genotypes without highly specific reagents (Al-Sunaidi et al., 2007; Drexler et al., 2009). This is especially useful in in vitro studies, where cross-reactivity can make it harder to interpret genotype-specific responses.

Thus, even though molecular methods may still seem to be the most reliable for detecting parechoviruses, there is a great need for antibody-based approaches to be improved to provide ease access alternative for research facilities that may not have access to sophisticated molecular tools. Most especially, VP0-targeting monoclonal antibodies offer a useful direction for broader detection (Tripathi et al., 2021a).

1.10 Parechovirus cultivation in cell lines

Human parechoviruses (PeV-A) have been cultivated in various cell lines since their early discovery, and most of the current knowledge of their biology comes from studies investigating cell susceptibility, replication efficiency, and antigen expression. In all these studies, it is evident that different PeV-A genotypes do not behave similarly, and that the origin and

characteristics of the host cell strongly influence how efficiently the virus can replicate and establish infection.

Early research focused primarily on PeV-A1 (Harris strain), which was shown to commonly replicate in used virology cell lines, such as A549, HeLa, and RD (Alho et al., 2003; Ito et al., 2004; Nix et al., 2008). These cells provided an important starting point for characterizing cytopathic effects and viral protein expression. However, PeV-A replication efficiency was not consistent across these models, suggesting that standard laboratory cell lines may not fully reflect the natural physiological environment suitable for these viruses. This led to increased interest in more physiologically relevant systems.

Subsequently, follow-up studies increased the range of susceptible cell types, illustrating that PeV-A1 can also infect intestinal epithelial cell lines such as HT-29 and Caco-2, as well as the neuroblastoma cell line SH-SY-5Y (Westerhuis et al., 2013). These studies began to highlight some key differences not only between cell lines but also in how replication is measured using molecular tools. For example, Westerhuis et al. (2013) used quantitative PCR to compare viral RNA levels and found that HT-29 and A549 supported stronger replication than Caco-2 and SH-SY-5Y. This suggests that both cell type and detection method used can influence how parechoviral growth is interpreted.

Moreover, PeV-A3 has provided more insight into the genotype-specific behaviour of these viruses. In contrast to PeV-A1, PeV-A3 has been reported to replicate most efficiently in Caco-2 and SH-SY-5Y cells, with lower replication rates in A549 and HT-29 (Westerhuis et al., 2013). This difference is important because it demonstrates that even closely related genotypes can show distinct cell-line preferences. More studies confirmed that PeV-A3 can infect Vero, HeLa, and LLC-Mk2 cells (Benschop et al., 2008; Ito et al., 2004), even though replication of these viruses in these non-intestinal lines is often less efficient and varies more. Recent studies have shown PeV-A3 to infect the human airway epithelial (HAE) models (Sridhar et al., 2019), suggesting that its tropism is not restricted to the gastrointestinal tract and may involve a much larger range of tissues.

Other genotypes, including PeV-A2, PeV-A4, and PeV-A6, have also been studied in different cell systems, although to a lesser extent. PeV-A2 has been successfully propagated in Vero cells (Ghazi et al., 1998; Ito et al., 2004), while PeV-A4 and PeV-A6 have been grown in LLC-Mk2 and HeLa cells (Benschop et al., 2008; Ito et al., 2010). Some comparative studies provide a more integrated view by examining multiple genotypes across several cell lines (Kolehmainen

et al., 2012). Findings from the study showed that HT-29 consistently supported replication of PeV-A1, A3, and A6, whereas more variable susceptibility was observed in VeroE6 and A549. This reemphasized the idea that intestinal epithelial cells offer a more suitable physiological environment for PeV-A growth and replication.

A more recent development in theis field is the use of HuTu80 cells, a human duodenal epithelial cell line, which is the basis of this study. This study demonstrated that HuTu80 can support the replication of PeV-A1 to A6, making it one of the few cell lines capable of supporting multiple genotypes in a more consistent manner (Takagi et al., 2022). The discovery of this cell line is particularly relevant given the gastrointestinal tropism of parechoviruses. Interestingly, the same study reported that HCT-8 cells did not support PeV-A3, despite also being of intestinal origin. This suggests that differences in receptor expression or intracellular factors between epithelial cell lines can significantly affect viral entry and replication.

As a result, these studies show that PeV-A can infect a large range of cell lines, including A549, HeLa, RD, Caco-2, SH-SY-5Y, Vero, VeroE6, LLC-Mk2, HT-29, and HuTu80. However, the efficiency of replication and the detectability of viral antigen greatly differ depending on both the genotype and the host cell. A very important pattern across the literature is that human intestinal epithelial cell lines, mostly HT-29 and HuTu80, tend to provide more reliable and biologically relevant models for studying PeV-A infection.

Hence, based on this background, the present study focuses on the growth characteristics and antibody-based detection of PeV-A types 1–6 in HuTu80 cells. While Takagi et al. (2021) established HuTu80 as a permissive system for multiple genotypes, there is still limited information on how antigen expression varies between genotypes or how effectively different antibodies detect infection in this model. In addition, direct comparisons with other intestinal cell lines, such as HT-29, remain limited.

By combining cytopathic effect analysis, immunofluorescence, RT-qPCR, ELISA, and quantitative image analysis, this study provides a more detailed and integrated assessment of PeV-A infection in HuTu80 cells. This approach not only allows confirmation of viral replication but also enables comparison of antigen expression and detection across genotypes. As such, it extends previous findings and contributes to a more comprehensive understanding of how different PeV-A types behave in a physiologically relevant intestinal model.

2. Aim and objectives

The study aims to investigate PeV-A infectivity in the HuTu80 cell line and visualize infection via immunofluorescence microscopy using parechoviral antibodies.

2.1 Hypotheses

HuTu80 cells are permissive to types 1 to 6 PeV-A virus, and immunofluorescence microscopy using parechoviral antibodies will provide a sensitive and specific method for visualizing PeV-A viral replication, with performance comparable to RT-qPCR and ELISA.

2.2 Objectives

The specific objectives of this study are as follows:

1. To evaluate whether HuTu80 cells support the replication of types 1- 6 parechovirus.
2. To optimize the detection of PeV-A-infected cell lines using different antibodies in an immunofluorescence assay.
3. To use RT-qPCR and ELISA methods as control methods to confirm virus replication in HuTu80 cells.
4. To analyze unknown clinical samples with parechoviral antibodies in HuTu80 cells.

3. Materials and methods

3.1 Cell lines

HuTu80, HT-29, and Vero E6 cell lines (obtained from ATCC), were used for the study. The cell lines were cultured in T75 tissue culture flasks with vent caps (Sarstedt AG & CO, Numbrecht, Germany) under standard conditions. HuTu80 cells were grown in Eagle's Minimum Essential Medium (EMEM) (Bio Whittaker, Walkersville, USA) supplemented with 10% fetal bovine serum (FBS) (Gibco, UK) and penicillin–streptomycin. While HT-29 and Vero-E6 cells were grown in Dulbecco's Modified Eagle's Medium (DMEM) (Bio Whittaker, Walkersville, USA) supplemented with 7% fetal bovine serum (FBS) (Gibco, UK), glutamax, and penicillin–streptomycin. The cell cultures were incubated at 37 °C in a humidified atmosphere containing 5% CO_2 in an incubator (Panasonic Healthcare, Co., Ltd., Indonesia). Cells were split twice a week.

3.2 Cell splitting

To maintain the cell line cultures, all cell lines were routinely passed twice weekly to prevent confluent overgrowth, ensure viability, and maintain optimal nutrient availability in the culture medium. However, before splitting, pre-warmed 10% FBS-supplemented EMEM and 7% FBS-supplemented DMEM were equilibrated in a 37 °C incubator, while phosphate-buffered saline (PBS; Hyclone Lab, Logan, Utah, USA) and 0.25% 1× Trypsin-EDTA (Gibco, Parkley, UK) were allowed to reach ambient temperature within a laminar flow cabinet (BioWizard Silver, Kojair Technologies Oy, Finland) to minimize thermal stress on cells.

For subculturing, spent medium was aspirated from culture flasks, and the monolayer was rinsed once with 10 mL PBS to remove cellular debris. Cells were then treated with 2 mL Trypsin-EDTA, gently swirled, and incubated for 3 minutes at 37 °C to promote detachment. Enzymatic activity was neutralized by adding 10 mL of fresh EMEM or DMEM, and the resulting suspension was triturated thoroughly to achieve a single-cell dispersion. Depending on the desired split ratio, 2-4 mL of the cell suspension was transferred into new flasks containing 20 mL of complete medium. Cultures were maintained at 37 °C in a humidified atmosphere of 5% CO_2. Note, HuTu80 cell growth efficiency was also monitored by comparing different serum concentrations of culture medium.

3.3 Cell counting

Following section 3.2, a 10 µL aliquot of the detached cells was mixed with an equal volume of trypan blue (Bio-Rad, USA). A 10 µL portion of this mixture was loaded into a dual-chamber cell counting slide (Bio-Rad Laboratories, USA) and analyzed using a TC20™ automated cell counter (Bio-Rad, Singapore). Next, 200 µL of the adjusted cell suspension was seeded into each well of three labeled 96-well plates (Greiner, Corning, and Sarstedt). The plates were gently swirled to ensure even cell distribution and incubated at 37 °C in a humidified 5% CO_2 atmosphere.

3.4 Infectivity test by CPE

The susceptibility of HuTu80 cells to *Parechovirus A* (PeV-A) infection was evaluated using a panel of 40 distinct PeV-A strains, representing virus types 1 through 6. The specific virus types and strains used in this study are summarized in Appendix 1. Firstly, HuTu80 cell growth characteristics were compared between three standard 96-well tissue culture plates: Greiner, Corning, and Sarstedt, and the best plate was used for analyses.

HuTu80 cells were seeded and allowed to reach an appropriate confluency by the following day. The growth medium was then aspirated using the suction machine (Vacuubrand Gmbh, Germany) and replaced with 100 µL of infection medium, consisting of Eagle's Minimum Essential Medium (EMEM) supplemented with 2% fetal bovine serum (FBS) and 1% penicillin–streptomycin. Infection was performed by adding 10 µL of each PeV-A viral stock to the wells containing HuTu80 cells. Following gentle pipetting to ensure homogeneous mixing, 10 µL of the resulting viral suspension was serially diluted ten-fold across subsequent wells down to the fourth row (row D), generating four wells containing sequential 10-fold virus dilutions.

The progression of viral infection was monitored at 24, 48, and 72 hours post-infection. Cellular morphology in infected wells was examined using both light (PrimoVert, ZEISS) and fluorescence microscopy (EVOS FL Imaging System) and compared with non-infected control wells to assess the presence of cytopathic effects (CPE). Morphological changes indicative of viral infection were documented, and representative images were acquired using ZEN digital imaging software (ZEISS) for subsequent analysis.

3.5 Antibodies

After CPE testing, IFA was used to confirm the presence of parechoviral antigen replication in HuTu80 cells. The following primary antibodies were used to detect parechovirus antigens: the mouse monoclonal antibody P5C4 and a panel of polyclonal antibodies (pAb), including pAb-K8873, -K8851, -K306, and -K316. To minimize nonspecific binding and reduce background fluorescence, all polyclonal antibodies were subjected to cell-affinity purification before use (section 3.5.1). In addition, the following single-chain variable fragments (scFv) antibodies were employed: scFv-55, scFv-59, and scFv-71.

3.5.1 Cell affinity purification of antibody

To reduce the non-specific background signal, the crude antiserum of all the polyclonal antibodies was pre-absorbed against the HuTu80 cells before use in immunoassays. Based on the original (crude) antiserum, a working antibody solution was prepared in phosphate-buffered saline (PBS) at a 1:5 (1+4) ratio to a final volume of 1 mL per 6-well plate. Specifically, 200 µL of antiserum was diluted in 800 µL of PBS.

Based on the count obtained as described in section 3.3, HuTu80 cells were seeded into 6-well plates at a final seeding density of 6 × 10 ^5 cells per well. For antibody purification, the culture medium was first removed from the culture cells. The prepared antibody solution was then added to the first well. The plate was incubated at room temperature (~20°C) for 1 hour on a gentle shaker or rotator to allow for binding.

Following incubation, the antibody-PBS solution was transferred sequentially to subsequent wells, repeating the incubation process in each. This absorption step was performed across 3 wells to deplete non-specific antibodies. After the final incubation, the antibody solution was collected and marked. The solution was filter-sterilized using a 0.22 µm filter. The tube was clearly labelled with the antibody dilution and stored at +4°C until required for use.

3.6 Cell fixation and immunofluorescence staining

Cells were seeded into a black 96-well microplate (Revvity (formerly PerkinElmer), cat. no. 6005050) at a density of 1.5×10^4 cells per well and incubated overnight to facilitate adherence and ensure isolated cell distribution for optimal single-cell imaging. Following attachment, cells were infected with 1 µL of the specified Parechovirus inoculum to initiate infection, which was subsequently increased to 10 µL of inoculum to increase the multiplicity of infection (MOI)

and enhance overall infectivity. Infected cultures were initially maintained for 24 hours at 37 °C in medium supplemented with 2% serum. However, to align with the short replication cycle of picornaviruses (PeVs), which can complete a single round of infection within several hours, subsequent infection periods were reduced to shorter durations of ≤6 hours for relevant experiments.

After the designated infection period, the medium was aspirated, and cells were fixed inside a fume hood using 100 µL of 4% paraformaldehyde (PFA) in phosphate-buffered saline (PBS) for 10–20 minutes at room temperature. Following fixation, cells were washed three times with PBS (5 minutes per wash under gentle agitation) and permeabilized with 100 µL of 0.1% Triton X-100 for 5–15 minutes. Subsequent steps were performed on the benchtop, as viral infectivity was eliminated.

After three additional PBS washes, cells were incubated for 1 hour at room temperature with 60 µL of virus-specific primary antibodies diluted to a minimum of 1:100 in 3% bovine serum albumin (BSA) in PBS. Following three PBS washes, cells were incubated with Fluorophore-conjugated Anti-Mouse/Rabbit IgG antibodies (Goat Anti-Mouse/Rabbit IgG-Alexa Fluor 488) diluted 1:400 in 3% BSA/PBS (100 µL per well) for 45–90 minutes at room temperature in the dark. Excess secondary antibody was removed by washing four times with PBS.

For nuclear counterstaining, a 1:1000 dilution of DAPI (1mg/ml) in 3% BSA-PBS was added (60 µL per well). Plates were incubated in the dark with gentle shaking for 5–10 minutes, protected from light with a cardboard cover, and then washed with PBS. Stained plates were stored in the dark (wrapped in aluminum foil) at 4 °C until imaging. Fluorescence images were captured using an EVOS FL fluorescence microscope with exposure times optimized per channel and kept constant across experimental conditions.

All primary antibodies were diluted 1:100 in bovine serum albumin (BSA) prepared in phosphate-buffered saline (PBS) unless otherwise stated. For immunofluorescence detection, the secondary antibodies used were Alexa Fluor–conjugated goat anti-mouse IgG (H+L) and goat anti-rabbit IgG (H+L) (Life Technologies, Thermo Fisher Scientific, GmbH; cat. no. A-11001). For detection of FLAG-tagged scFv antibodies, a rabbit anti-FLAG antibody (Cell Signaling Technology, cat. no. 2368) was used at a dilution of 1:400.

3.7 Viral RNA extraction

I decided to proceed to confirm whether I have viral RNA in the PeV-A-infected HuTu80 cells using RT-qPCR, which requires RNA isolation. To collect samples for RNA extraction, cells were initially seeded into well plates at a density of 30,000 cells per well as described in section 3.3. Twenty-four hours post-seeding, the culture medium was removed, and cells were infected with 10 µl of viral inoculum (20 different strains of PeVs type 1-6). Following a two-hour adsorption period at 37°C, the inoculum was aspirated, and cells were gently washed three times with 200 µl of phosphate-buffered saline (PBS) per well; similarly, this procedure was also performed for non-infected control wells.

After the final wash, 100 µl of fresh medium supplemented with 2% fetal calf serum (FCS) was added to each well, and the culture was returned to incubation. Plates were monitored for 24 hours and 48 hours for the appearance of cytopathic effects (CPE). Upon observation of characteristic CPE, a representative well was documented by microscopy, and the sample was harvested by gently scraping the cells and transferring the contents to a pre-labeled 1.5 mL microcentrifuge tube. All collected samples were clearly marked with their unique sample ID and stored at -80°C for subsequent analysis.

RNA was isolated using the EchoLUTION^{TM} Viral RNA/DNA Kit. Before use, the column matrix was homogenized by vortexing and allowed to stand to remove air bubbles. The spin column was prepared by snapping off the bottom cap and equilibrating the column by centrifugation (Eppendorf AG centrifuge, Hamburg, Germany). Previously prepared PeV-A samples were lysed by mixing 50 µl of each sample with 50 µl of LyseNact® Buffer New Formula (BioEcho Life Science GmbH, Cologne, Germany), and PeV-A control samples were also included, followed by vortexing to release viral particles. A total of 100 µl of the lysed sample mixture was then slowly applied to the middle of the spin column, and the column with the cap opened half a turn was centrifuged at 1000 g (RCF) for 1 min at RT (to allow binding of viral RNA). After centrifugation, the flow-through containing purified viral RNA was collected and stored at -80°C for RT-qPCR application.

3.8 RTq-PCR

Following parechoviral RNA isolation, I performed the RT-qPCR to quantify the viral RNA by monitoring fluorescence signals generated during amplification. The reaction master mix was prepared using RNase-free H_2O (Invitrogen, Life Technologies Ltd, Paisley, UK), 2×SensiFAST mix (Meridian Bioscience), 10 µM each of the forward and reverse primers, PAR-F and PAR-R (5′-CTTATGCYCACACAGCCATCC, 319-340 nt and 5′-GGTACCTTCTGGGCATCCTTC 595-575 nt), and reverse transcriptase (Meridian Bioscience), scaled according to the total number of samples to be analyzed (Benschop, Molenkamp, et al., 2008; Österback et al., 2013). In vitro transcription (IVT) control stock (5.3×10^{11} copies/µL) was serially diluted as required by the protocol to generate working concentrations ranging from 1×10^6 to 1×10^1 copies/µL. For plate setup, 18 µL of master mix was aliquoted into designated MIC tubes, followed by the addition of 2 µL of extracted viral RNA, non-infected HuTu80 cell control, or diluted IVT control. All tubes were clearly labeled, securely capped, and loaded into a MIC-PCR system programmed with cycling conditions optimized for parechovirus detection (see table below). The run was executed according to the established program.

Table 1: MIC run program (one step)

RT step:	
+ 45°C	10 min (RT-step)
+ 95°C	2 min (inactivation of PCR enzyme)
3-step PCR cycling:	
+ 95°C	15 s – denaturation
+ 65°C -> 56°C	20 s - annealing (Touchdown: from 65 °C to 56°C during the first 9 cycles), then 41 cycles (50 cycles in total)
+ 72°C	10 s (signal generation FAM)
+ 72°C	95 °C - melt (1.5 °C/s; 72°C => 95°C)

3.9 ELISA

A solid-phase immunoassay was performed to detect viral antigen using a streptavidin-coated microtitration plate (Kaivogen, Cat: 41-04, Lot: KG2738) and biotinylated monoclonal antibodies. Parechovirus samples (20 isolates) exhibiting cytopathic effects for 24 to 48 hours were used as analytes. The assay used biotinylated anti-VP0 monoclonal antibody P5C4 and horseradish peroxidase (HRP)-conjugated anti-VP0 monoclonal antibody P5C4 as detection reagents. All wash steps were performed using PBS-T (PBS containing 0.05% Tween-20), and 1% bovine serum albumin (BSA) in PBS-T served as the blocking and diluent buffer. The enzymatic reaction was developed with a tetramethylbenzidine (TMB) substrate solution (TMB ONE, Kementec Solutions #4380A) and stopped with 0.2 M sulfuric acid.

The assay procedure began by pre-washing the streptavidin plate. Subsequently, 100 µl of biotinylated P5C4 antibody, diluted to a working concentration of 5 µg/ml and 2.5 µg/ml in 1% BSA/PBS-T, was added to each well and incubated for 30 minutes at room temperature with gentle agitation. After three washes, 80 µl of blocking buffer was added to each well. The plate was then transferred to a virus laboratory laminar flow hood, where 20 µl of virus-infected samples were added per well, followed by a one-hour incubation.

Following three subsequent washes, 100 µl of HRP-conjugated P5C4 antibody, diluted to 5 µg/ml, was applied and incubated for 1 hour at room temperature with agitation. After a final wash cycle, 100 µl of TMB substrate (Thermo-Fisher, USA) was added per well, and the plate was incubated in the dark for 15 minutes. The reaction was terminated by adding 100 µl of 0.2 M H_2SO_4 per well. The optical density at 450 nm (OD450) was measured immediately to quantify the signal.

3.10 Parallel IFA and image analysis

To compare the effectiveness of our IFA protocol on detecting PeV-A1 to A6 in HuTu80 cells, we decided to perform parallel IFA using HuTu80 and other commonly used cell lines, HT-29 and VeroE6. The IFA was performed using the same experimental conditions as described in sections 3.3 and 3.6. Afterwards, representative images were analyzed to calculate the infection rate in different cell lines.

Representative fluorescence images were analysed in Fiji/ImageJ using a consistent workflow to count total cells and identify infected ones in all images. The images were first separated into

two channels: blue (DAPI) for nuclei and green for PeV-A viral antigen. The DAPI channel was used to count the total number of cells. After that, the background signal was reduced using the Subtract Background function, followed by thresholding to clearly identify the nuclei. Then, a watershed step was applied to separate touching nuclei, and cells were counted using the Analyze Particles tool, with settings performed to exclude debris.

The same steps were performed on all green channels to detect viral antigen. After background removal and thresholding, the green signal was converted into a binary mask. To identify infected cells, this mask was combined with the nuclei image so that only nuclei overlapping with the viral signal were selected. These overlapping cells were then counted as infected cells using the same analysis settings. Finally, the infection rate for each image was calculated as the number of infected cells relative to the total number of cells.

4. Results

I performed a preliminary test to check the best 96-well culture plates to use for the virus infectivity test based on CPE. Based on the seeding and culturing of HuTu80 cells as described in section 3.3, cell growth characteristics were compared between three 96-well tissue culture plates: Greiner, Corning, and Sarstedt. The Sarstedt plate demonstrated the most favorable growth conditions based on subjective observation. Cells on this plate were well dispersed, a prerequisite for optimal testing, demonstrating that Sarstedt plates supported the optimal HuTu80 cell distribution. The cells cultured in Sarstedt plates showed a uniform, even spread across the entire well surface.

In contrast, cultures in Greiner and Corning plates exhibited pronounced edge-clustering, indicating suboptimal surface characteristics or well geometry for this cell line. Additionally, HuTu80 cell growth was evaluated in EMEM supplemented with 5% and 10% fetal bovine serum (FBS). Cells cultured in 10% FBS-EMEM displayed visibly improved morphology, higher viability, and faster proliferation. Although HuTu80 cells survived in 5% FBS-EMEM, long-term culture under reduced-serum conditions resulted in significantly lower cell densities and diminished overall growth performance.

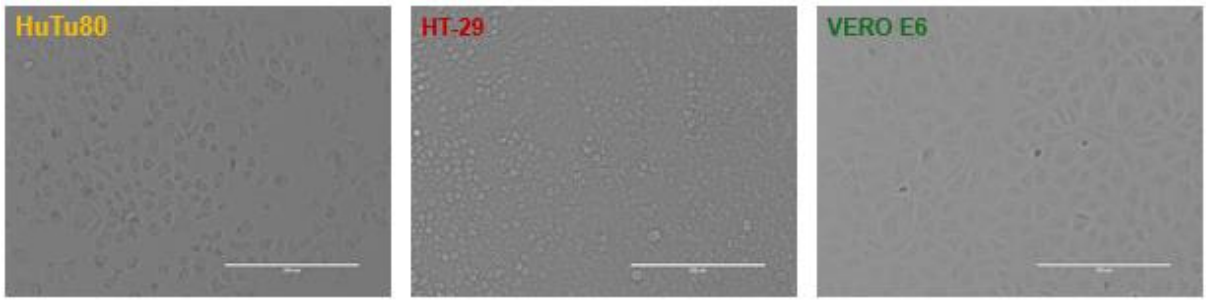

Figure 5: Morphology of HuTu80, HT-29, and VERO E6 cell lines. Representative brightfield images of HuTu80, HT-29, and VERO E6 cells cultured in T75 flasks. Cells were maintained in complete growth medium and imaged at 70–80% confluency using a 20x objective. Scale bar represents 200 µm. Images were captured using the EVOS FL digital inverted microscope.

4.1 Preliminary testing of PeV-As on HuTu80 cells for CPE

At the early stage, I wanted to confirm that the HuTu80 cells were permissive to PeVs by performing the infectivity test as described in section 3.4. Initially, I infected HuTu80 cells with 20 different strains of PeV-As, types 1 to 6, and assessed infectivity based on CPE observed at 1, 2, and 3 days post-infection because the infection dose was unknown. The cytopathic effects

(CPE) observed in HuTu80 cells following infection with PeV-A strains (types 1–6) at 1, 2, and 3 days post-infection (DPI) are presented in Table 2. Overall, the table demonstrates clear time- and strain-dependent cytopathic effects in HuTu80 cells following PeV-A infection. However, most of the PeV-1, PeV-3, and PeV-4 strains induced detectable CPE as early as 1 DPI, with severity increasing by 2–3 DPI, indicating rapid viral replication and high cell susceptibility. In contrast, some PeV-2, PeV-5, and PeV-6 strains showed delayed or weak CPE, with minimal or no effects observed at early time points and gradual progression at later DPI. A small subset of strains failed to induce CPE at 2 DPI, suggesting lower infectivity or slower replication kinetics in HuTu80 cells.

Table 2: CPE caused by some PeV-A types and isolates in HuTu80 cells. This table is a summary of clear strain- and time-dependent CPE patterns, with parechovirus A1, A3, and A4 inducing early and progressively severe CPE, while many PeV A2, A5, and A6 strains showed delayed, weak, or absent CPE, indicating slower replication or lower infectivity in HuTu80 cells.

	VT		W1	W2	W3		VT		W1	W2	W3
1DPI	PeV-1	Harris	++++	++++	++++	1DPI	PeV-1	50112 04759	-	-	-
2DPI			++++	++++	++++	2DPI			+	+	-
3DPI			++++	++++	++++	3DPI			++	++	+
1DPI	PeV-3	145-8	+++	++	+	1DPI	PeV-1	5068704768	-	-	-
2DPI			++++	+++	++	2DPI			-	-	-
3DPI			++++	+++	+++	3DPI			-	-	-
1DPI	PeV-1	153-20	+++	++	+	1DPI	PeV-1	50177 4432	-	-	-
2DPI			+++	+	+	2DPI			-	-	-
3DPI			++++	++	++	3DPI			-	-	-
1DPI	PeV-1	150-8	+++	++	++	1DPI	PeV-1	5050404763	-	-	-
2DPI			+++	+++	+++	2DPI			-	-	-
3DPI			++++	++++	++++	3DPI			+	-	-
1DPI	PeV-1	145-12	+++	+++	++	1DPI	PeV-1	5058104764	+	+	-
2DPI			++++	++++	+++	2DPI			+	++++	-
3DPI			++++	+++	++++	3DPI			++	++++	+
1DPI	PeV-1	125-7	+++	+	+	1DPI	PeV-3	A308/99	++++	++++	+++
2DPI			+++	++	++	2DPI			++++	++++	++++
3DPI			+++	+++	+++	3DPI			++++	++++	++++
1DPI	PeV-1	103-2	+++	++	++	1DPI	PeV-3	88	++	+	+
2DPI			+++	+++	+++	2DPI			++++	++++	+
3DPI			++++	++++	+++	3DPI			++++	++++	++
1DPI	PeV-2	Williamson	+++	++	+	1DPI	PeV-3	K251181-02	++++	+++	+++
2DPI			+++	++	+	2DPI			++++	++++	++++
3DPI			++++	+++	++	3DPI			++++	++++	++++
1DPI	PeV-2	Williamson (1964 HeLa)	++	++	+	1DPI	PeV-3	145(8)	++	+	-
2DPI			++	++	+	2DPI			+++	+	-
3DPI			++++	+++	+++	3DPI			++++	++	+
1DPI	PeV-4	FI121236	++++	+++	+++	1DPI	PeV-3	K251181-02	+++	+++	++

2DPI			++++	++++	++++	**2DPI**			++++	++++	++++
3DPI			++++	++++	++++	**3DPI**			++++	++++	++++
1DPI	**PeV-3**	**88**	++	+	+	**1DPI**	**PeV-3**	**K251181-02**	++++	+++	++
2DPI			++++	++++	++++	**2DPI**			++++	++++	+++
3DPI			++++	++++	++++	**3DPI**			++++	++++	++++
1DPI	**PeV-4**	**20152401**	++++	++++	+++	**1DPI**	**PeV-3**	**3 (252277)**	+++	+	+
2DPI			++++	++++	++++	**2DPI**			++++	++++	+++
3DPI			++++	++++	++++	**3DPI**			++++	++++	+++
1DPI	**PeV-6**	**89**	+	-	-	**1DPI**	**PeV-3**	**4 (252277)**	+++	++	++
2DPI			++++	+++	++	**2DPI**			++++	++++	++++
3DPI			++++	++++	++	**3DPI**			++++	++++	++++
1DPI	**PeV-5**	**20552323**	++	-	-	**1DPI**	**PeV-2**	**Williamson**	++++	+++	++
2DPI			++++	+++	++	**2DPI**			++++	++++	++++
3DPI			++++	++++	+++	**3DPI**			++++	++++	++++
1DPI	**PeV-6**	**21152464**	+++	+++	++	**1DPI**	**PeV-2**	**Williamson**	-	-	-
2DPI			++++	++++	++++	**2DPI**			++++	+++	-
3DPI			++++	++++	++++	**3DPI**			++++	++++	+
1DPI	**PeV-5**	**20552322**	++++	++++	++++	**1DPI**	**PeV-6**	**2005-823**	-	-	-
2DPI			++++	++++	++++	**2DPI**			+++	++	+
3DPI			++++	++++	++++	**3DPI**			++++	++++	++
1DPI	**PeV-4**	**K251176**	++++	+++	+++	**1DPI**	**PeV-6**	**47**	-	-	-
2DPI			++++	++++	++++	**2DPI**			++	+	+
3DPI			++++	++++	++++	**3DPI**			++++	++	+
1DPI	**PeV-3**	**252277**	+	-	-	**1DPI**	**PeV-5**		++	+	-
2DPI			+	-	-	**2DPI**			++++	++++	+++
3DPI			++++	++++	++	**3DPI**			++++	++++	++++
1DPI	**PeV-3**	**152037**	++++	++++	+++	**1DPI**	**PeV-4**	**K251176**	++++	+++	++
2DPI			++++	++++	++++	**2DPI**			++++	++++	++++
3DPI			++++	++++	++++	**3DPI**			++++	++++	++++
1DPI	**PeV-3**	**K251181-02**	++++	+++	++	**1DPI**	**PeV-2**	**Williamson**	++++	+++	++
2DPI			++++	++++	+++	**2DPI**			++++	++++	++++
3DPI			++++	++++	++++	**3DPI**			++++	++++	++++

Note, infection was assessed in three replicate wells (W1–W3) and scored subjectively from no detectable effect (–) to strong CPE (++++) to compare strain- and time-dependent cytopathogenicity. W1 = 10 ul of virus, W2 = 1:10 dilution, and W3 = 1:100 dilution. VT = Virus type.

After the preliminary test, representative PeV-A genotypes with the strongest and earliest CPE were selected and tested for CPE at different concentrations, as shown in Figure 6. A clear dose-dependent cytopathic effect (CPE) was observed. The results show that 10 μL of viral inoculum results in extensive monolayer disruption, pronounced cell rounding, and detachment; 1 μL shows moderate CPE with partial loss of monolayer integrity; and 0.1 μL induces only mild morphological alterations.

At lower volumes, the changes were less obvious or appeared more slowly, and some differences were seen between genotypes. The uninfected control shows a confluent, morphologically intact monolayer. Because I performed titration at different viral volumes to visualize CPE and not cytotoxic effect, these images collectively propose parechovirus infection in HuTu80 cells.

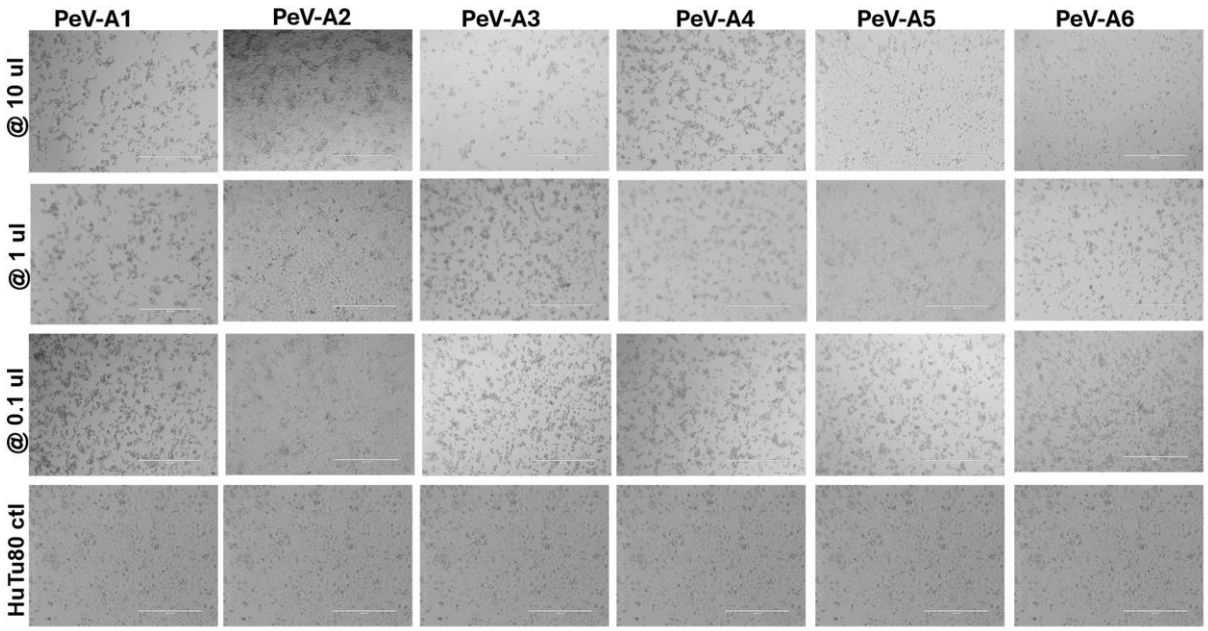

Figure 6: Representative images of HuTu80 cells infected with parechovirus types PeV-A1 to PeV-A6 at three inoculum volumes (10 µL, 1 µL, and 0.1 µL). Viral inoculum was serially diluted starting at 10 µL, then 1 µL, and finally 0.1 µL. Cytopathic effects (CPE) were examined 24 hours after infection using an EVOS microscope equipped with a 10X objective.

4.2 Immunofluorescence assay

After confirming that HuTu80 cells support infection with PeV-A types 1–6 through the observation of clear and reproducible cytopathic effects, an immunofluorescence assay (IFA) was performed to detect viral antigen expression and visualize the location of infection within the cells. Given that PeV-A types 1-6 induced pronounced cytopathic alterations in the morphological architecture of HuTu80 cells, representative strains from each PeV-A type (as shown in Appendix 2) exhibiting the most rapid onset of CPE were selected for subsequent experiments.

At 6 hours post-infection, the cells were fixed and stained for viral antigen (green), while the nuclei were counterstained with DAPI (blue). This allowed viral proteins to be detected in

infected HuTu80 cells using the monoclonal antibody P5C4 together with a panel of polyclonal antibodies (Appendix 3). The assay also made it possible to observe differences in antigen distribution between genotypes at the single-cell level.

To identify a suitable inoculum volume for antibody-based detection, all six PeV-A genotypes were first tested in a preliminary IFA experiment. Using 1 µL of inoculum resulted in only a few antigen-positive cells, suggesting that the viral input was too low for clear detection (Figure 7). As part of the assay validation, the monoclonal antibody J2 was used as a positive control for viral dsRNA detection. J2 produced a clear fluorescence signal in infected cells, confirming active viral replication, while the uninfected HuTu80 control cells showed only DAPI-stained nuclei, confirming the specificity of the staining.

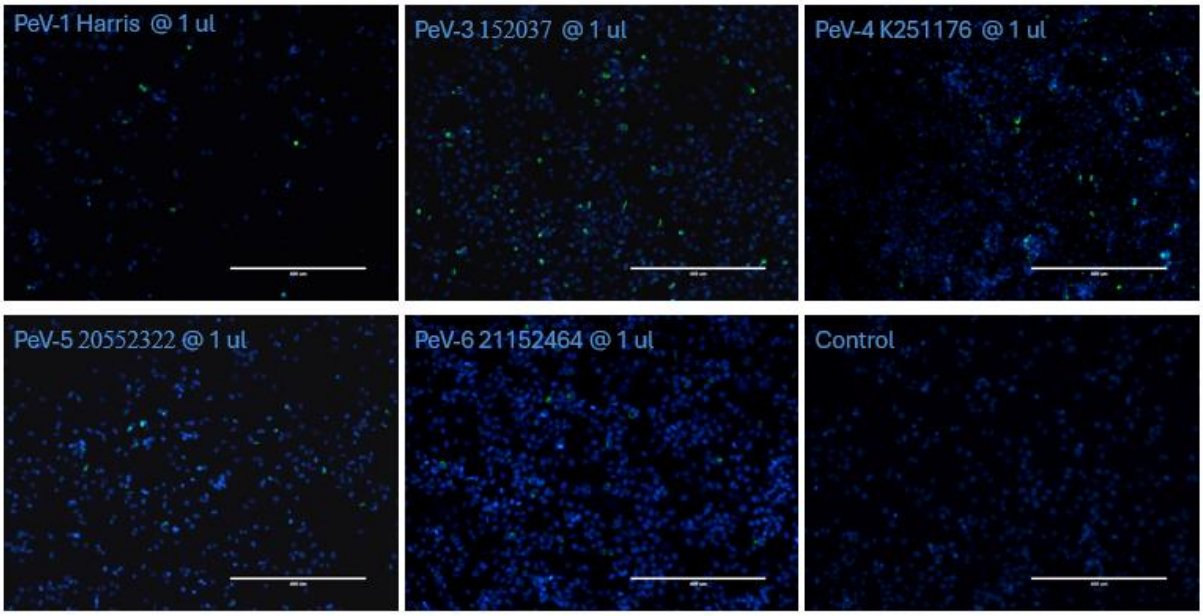

Figure 7: Representative immunofluorescence images of PeV-A–infected HuTu80 cells at 1 µL inoculum. Images were taken with the EVOS microscope using a 10x objective at 6 hours post-infection. PeV-A-infected cells fixed and stained with 22ug/ml P5C4 show the presence of viral antigen (green) and counterstained with DAPI to visualize nuclei (blue). The uninfected control shows only nuclear staining without a detectable viral signal, confirming staining specificity.

Because antigen detection at 1 µL was limited, higher inoculum volumes were tested to improve signal detection. As the inoculum increased, the fluorescence signal also increased, showing that a higher viral dose resulted in greater viral antigen detection in infected cells (Figure 8). Different concentrations of the P5C4 antibody were also tested to optimize the staining

conditions. A stronger fluorescence signal was observed at 44 µg/mL than at 22 µg/mL, indicating that the higher antibody concentration improved detection under the conditions used.

The IFA results showed differences in infection patterns between the genotypes. PeV-A1 (Harris), PeV-A3 (3152037), and PeV-A4 (K251176) showed strong and widespread fluorescence across the cell monolayer, indicating efficient infection, with PeV-A3 and PeV-A4 showing the highest number of antigen-positive cells. PeV-A5 (20552322) showed moderate staining, while PeV-A6 (21152464) showed fewer antigen-positive cells and mainly nuclear staining, which may indicate lower replication efficiency or reduced antigen detection at this time point. As expected, the uninfected control showed only DAPI-stained nuclei with no viral signal.

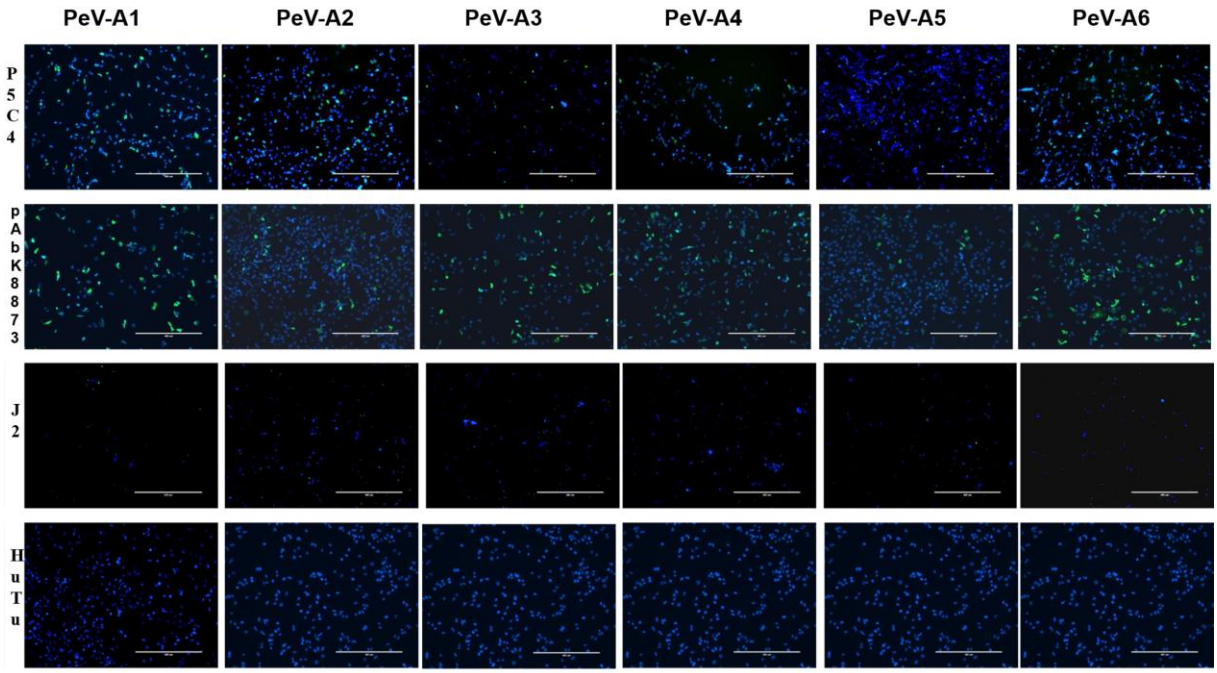

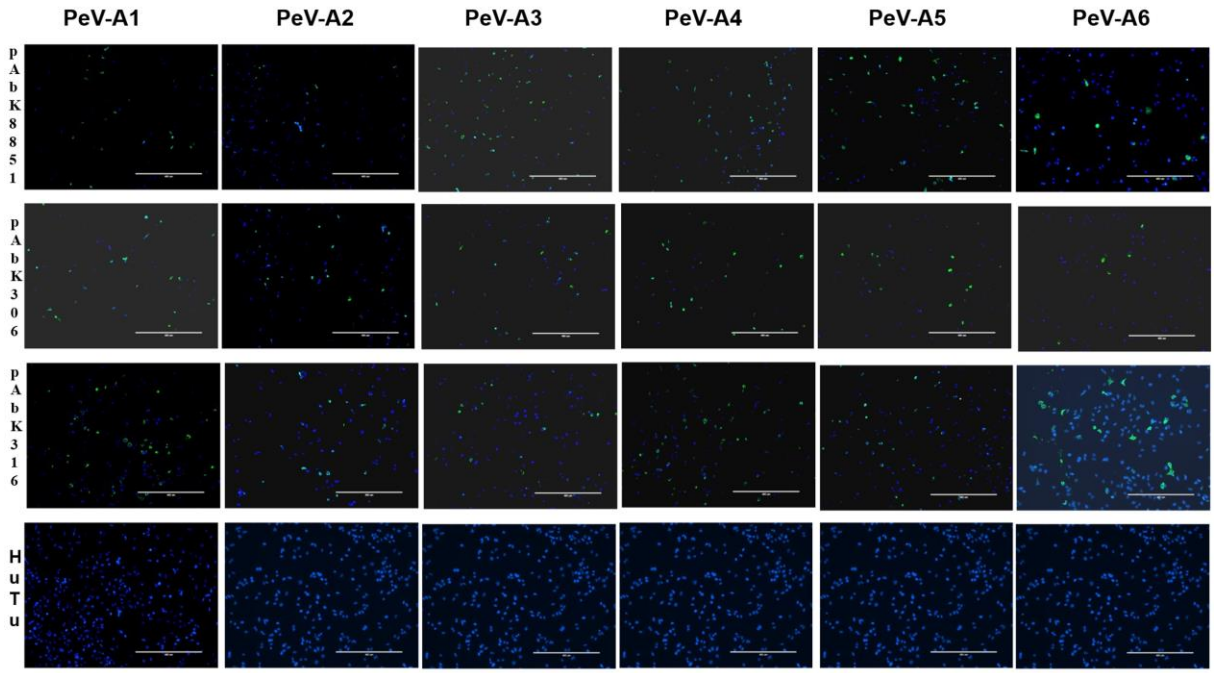

Figure 8. Immunofluorescence detection of HuTu80 cells infected with PeV A1 to PeV A6 using antibody preparations. Images were taken with the EVOS microscope using a 10x objective at 6 hours post-infection with 10 µL of each PeV-A genotype. PeV-A-infected cells fixed and stained with 44 µg/mL P5C4, cell-affinity-purified pAbs, and monoclonal antibody J2 show the presence of viral antigen (green) and counterstained with DAPI to visualize nuclei (blue). The uninfected control shows only nuclear staining without a detectable viral signal, confirming staining specificity.

Based on these optimization experiments, an inoculum volume of 10 µL and a P5C4 concentration of 44 µg/mL were selected for all subsequent analyses. This combination consistently produced strong and well-defined fluorescence signals with low background and performed better than the polyclonal antibody preparations in terms of specificity. Using these conditions, additional PeV-A1 to PeV-A6 strains from different sources were screened. More than 25 isolates showed positive reactivity with P5C4, supporting its usefulness for detecting a wide range of parechovirus genotypes (Appendix 4). In contrast, clinical samples collected in 1994, previously classified as Echovirus 22, did not show any reactivity with P5C4. This may be suggestive of their known antigenic differences from more recent PeV-A1 strains.

The reactivity of crude polyclonal antibody preparations was also tested in infected HuTu80 cells. However, the crude antibodies produced high background staining and low specificity, making them unsuitable for reliable detection. To improve performance, the polyclonal antibodies were further purified using cell-affinity purification. This reduced the background staining and improved the clarity of the fluorescence signal. After purification, differences in staining intensity were still observed between genotypes and antibodies, reflecting differences

in viral replication as well as variation in antibody reactivity.

The single-chain variable fragment (scFv) antibodies (scFv-55, scFv-59, and scFv-71) were included in this study (Table 3) to explore whether smaller, recombinant antibody formats could be used as an alternative for antigen detection, potentially offering better access to epitopes and lower background than full-length antibodies. However, none of the scFv preparations produced detectable fluorescence signals in PeV-A–infected HuTu80 cells. This lack of signal may be due to low binding affinity or loss of proper epitope recognition during expression and purification. As a result, the scFvs were not suitable for antigen detection under the conditions used in this study.

Table 3: Antibody performances across PeV genotypes (A1-A6) in HuTu80 cells. The panel includes PeV-A types 1 to 6 and monoclonal antibody P5C4, four cell-affinity-purified polyclonal antibodies (pAb K8873, K8851, K306, and K316), and three single-chain variable fragments (scFv-55, scFv-59, and scFv-71). Reactivity (+/-) was assessed based on the presence or absence of viral antigen-associated fluorescence at 6 hours post-infection.

Antibodies	PeV-A1	PeV-A2	PeV-A3	PeV-A4	PeV-A5	PeV-A6
mAb P5C4	+	+	+	+	+	+
pAb K8873	+	+	+	+	+	+
pAb K8851	+	+	+	+	+	+
pAb K306	+	+	+	+	+	+
pAb K316	+	+	+	+	+	+
scFv 55	-	-	-	-	-	-
scFv 59	-	-	-	-	-	-
scFv 71	-	-	-	-	-	-

4.3 Verification of parechovirus infection in HuTu80 cells by RT-qPCR

To independently verify the presence of viral infection and quantify viral replication across the PeV-A genotypes, RT-qPCR was performed on RNA extracted from HuTu80 cells infected with selected PeV-A1 to PeV-A6. This helped to support and validate the findings obtained from the immunofluorescence experiments and whether there were viral antigens in PeV-A types and strains that did not show CPE. This analysis enabled the assessment of viral RNA levels in infected samples and provided quantitative confirmation of viral replication. By comparing Ct values and calculated viral genome copy numbers across isolates and controls, RT-qPCR served as a critical method to validate the presence and

abundance of PeV-A RNA and to support IFA analyses involving antibody-based detection and visualization of viral infection.

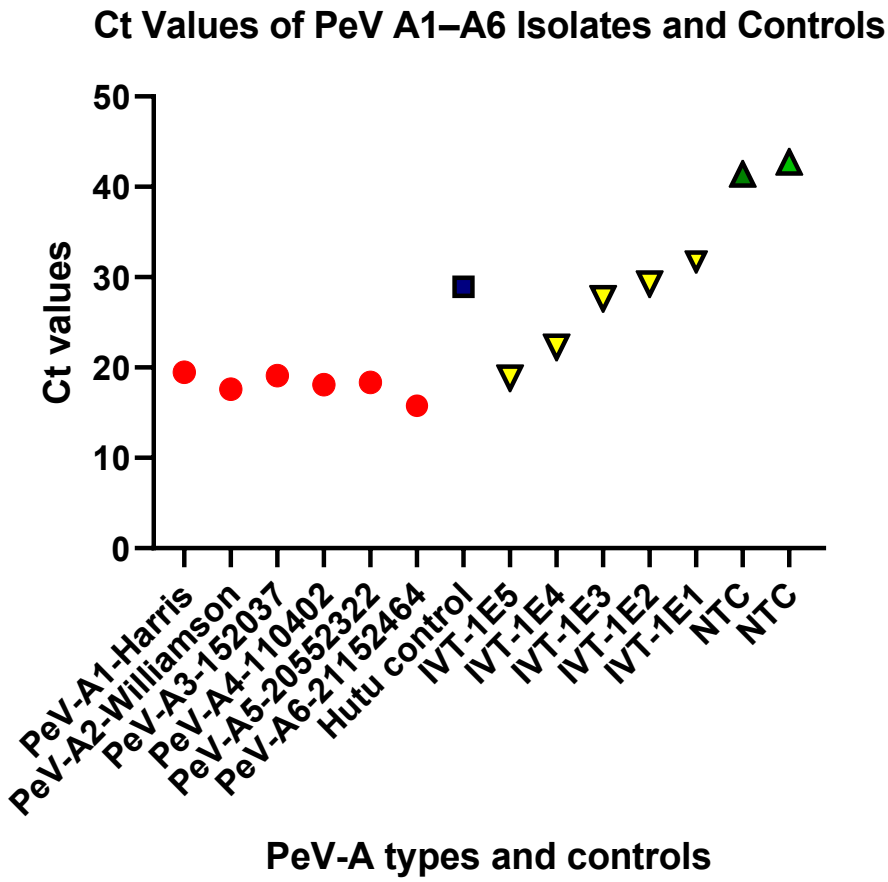

Figure 9: Quantification of viral RNA from representative PeV A1–A6 isolates by RT-qPCR, expressed as Ct values for each isolate. Scatter plots show cycle threshold (Ct) values for individual PeV isolates (PeV-A1 to PeV-A6) and experimental controls. Each dot corresponds to a single measurement.

My results show that all six isolates produced low Ct values clustered around and/or below 20, indicating high viral RNA abundance and confirming productive infection across genotypes (Figure 9). In contrast, the HuTu80 mock control generated a significantly higher Ct value of about 30, reflecting background signal in the absence of viral RNA (~80–122 copies/µL). The IVT RNA standards (10^5 to 10^1 copies) showed the expected stepwise increase in Ct values, validating the assay performance and sensitivity and confirming IVT RNA amplification efficiency.

Quantification of viral genome copy numbers further supported these findings (Appendix 6). Ct values for clinical isolates range from 15.10 to 29.09, corresponding to calculated concentrations from approximately 1.09×10^2 to 2.17×10^6 copies/µL. Most samples cluster

between 10^5 and 10^7 copies/µL, indicating moderate-to-high viral loads. The highest concentrations were observed in PeV-A1 isolate 145-12 (2.17×10^6 copies/µL) and PeV-A6 isolate 21152464 (1.30×10^6 copies/µL), both associated with low Ct values (~15–16). In contrast, two PeV-A3 samples (C2 and D4) showed very low concentrations (295 and 109 copies/µL) and high Ct values (~28–29), consistent with low template abundance.

Meanwhile, the HuTu80 control showed a low background signal, while non-template controls (NTCs) showed very late amplification with negligible copy numbers (<0.02 copies/µL). Also, lower IVT standards showed significantly reduced concentrations (Appendix 6). The reduction in genome copy numbers across the IVT dilution series confirmed the linear performance of the assay and supported accurate estimation of viral loads in the test samples. Amplification efficiencies ranged from 0.82 to 0.99 (82–99%). Most samples were within or close to the acceptable range of 90–110%, although a few lower values (e.g., 0.82–0.88) suggest slightly reduced efficiency. Despite this, the high R^2 values (0.99963–1.000) show good linearity of the standard curve and support reliable quantification.

As a result, the RT-qPCR results provide strong molecular evidence of viral replication in HuTu80 cells infected with PeV-A1 to PeV-A6. The high levels of viral RNA detected across all isolates support the immunofluorescence findings and confirm the presence of viral antigen, even in cases where cytopathic effects or fluorescence signals were less clear. This additional validation strengthens the reliability of the IFA-based detection and supports further comparison of infection patterns among the different PeV-A genotypes.

4.4 ELISA-based evaluation of P5C4 binding to PeV-A1 to PeV-A6

The ELISA assay was carried out to quantitatively assess the optimal concentration and binding specificity of the anti-PeV antibody to PeV-A viral antigens and to support our findings from the earlier CPE, IFA, and RT-qPCR assays.

The result of ELISA comparing P5C4 binding at 2.5 µg/ml and 5 µg/ml showed that the antibody successfully detected antigen from PeV-A1 to 6 types, with higher absorbance values observed at the 5 µg/ml concentration (Figure 10). This result shows stronger binding when the antibody concentration is increased. Although the exact absorbance varied between isolates, the result shows that P5C4 recognizes a wide range of PeV-A strains. Some isolates produced higher signals than others; this suggests differences in accessibility and presence of antigen or viral epitope. However, all tested types showed a slightly measurable binding effect above

background.

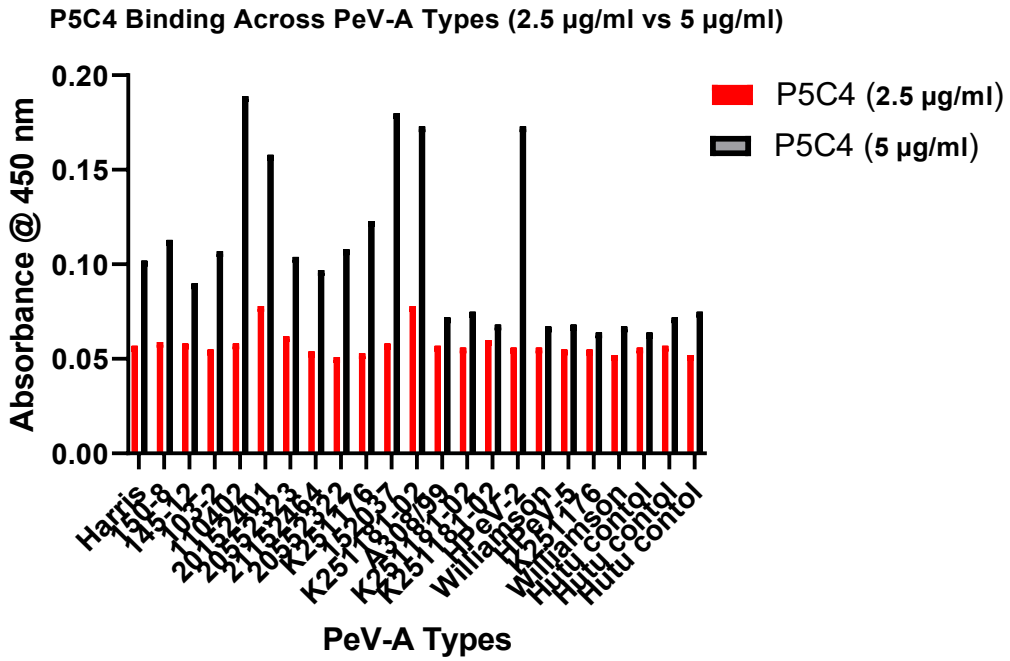

Figure 10. ELISA measurement of P5C4 binding to PeV A types at 2.5 µg/ml and 5 µg/ml. Absorbance at 450 nm was measured to compare antibody reactivity with the PeV-A isolates. For all tested genotypes, the 5 µg/ml concentration gave a higher absorbance than 2.5 µg/ml, indicating stronger binding at the higher antibody level.

In addition, Figure 11 showed that P5C4 binds specifically to the biotinylated PeV-A1 VP0 antigen in a concentration-dependent manner. As the antibody concentration increased, the absorbance at 450 nm also increased. But the controls, biotinylated GST and 1% BSA/PBS, showed only very low absorbance across all concentrations, indicating that the signal observed with VP0 was due to specific antigen–antibody binding and not nonspecific interactions.

The assay also showed that at lower P5C4 concentrations, the signal was weak, while at intermediate and higher concentrations, the absorbance increased and eventually reached saturation, as seen in the curve. This pattern thus indicates that the ELISA was both sensitive and specific, and able to clearly differentiate true antigen binding from background signal.

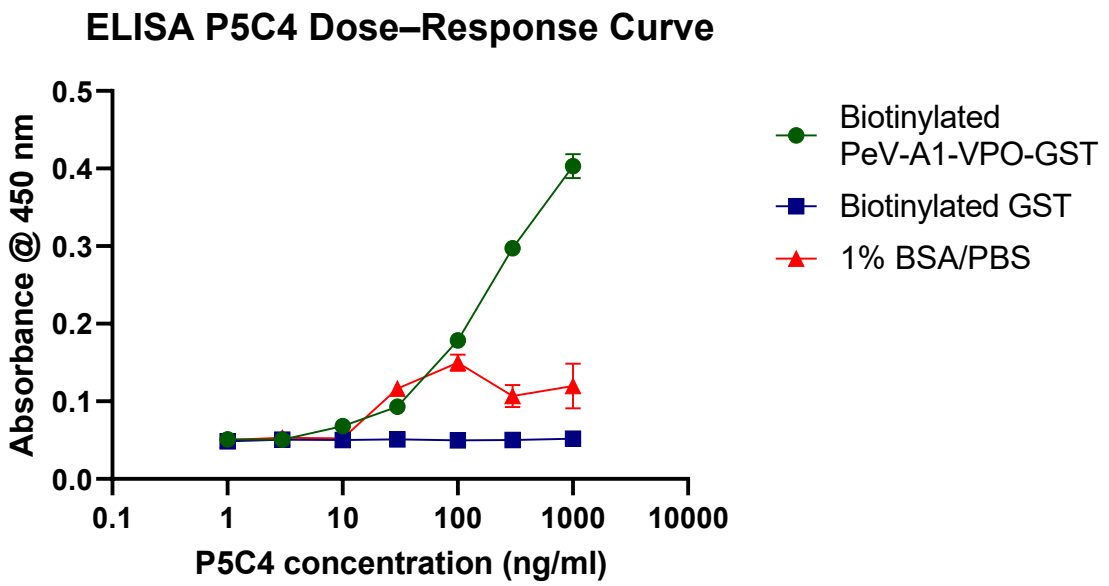

Figure 11: ELISA showing binding of P5C4 to PeV-A1 VP0 antigen. P5C4 was tested over a wide concentration range (0.1–10,000 ng/ml). Absorbance at 450 nm increased with increasing antibody concentration for the VP0 antigen. In contrast, the control dilutions (biotinylated GST and 1% BSA/PBS) showed only negligible absorbance at all concentrations, indicating that P5C4 binding to VP0 was specific.

4.5 Comparison of PeV-A infectivity and detection in HuTu80, HT-29, and VeroE6

Since I aimed to compare how human parechoviruses types 1 to 6 replicate in HT-29 and VeroE6 and can be visualized with P5C4, we performed a similar experiment as described in section 3.10. Representative fluorescence microscopy images of HT29 cells infected with the six PeV-A genotypes showed similar viral antigen detection signal patterns after 6 hours post-infection, while images of VeroE6 showed high background noise. Also, some images from VeroE6 appeared completely blurry, as though cells were absent, with no distinction between the DAPI and GFP channels. This may indicate that VeroE6 cells were not compatible with these IFA conditions or protocol.

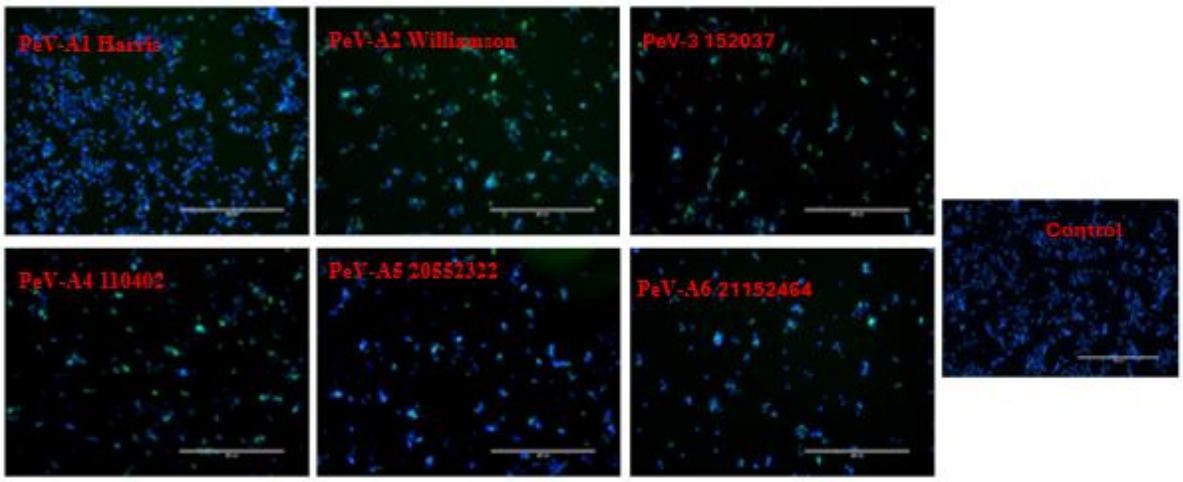

Figure 12: Detection of PeV-A infection in HT-29 cells by immunofluorescence. HT 29 cells were infected with the indicated PeV A genotypes and stained 6 hours post-infection using the P5C4 monoclonal antibody. Images were taken with the EVOS microscope using a 10x objective. Blue fluorescence represents DAPI-stained nuclei, while green fluorescence indicates viral antigen.

In HT-29 PeV-A-infected cells, the DAPI-stained nuclei appeared as blue signals, confirming intact cell monolayers under IFA conditions (Figure 12). The green fluorescence, representing viral antigen detected by the P5C4 monoclonal antibody, varied between PeV-A genotypes. Signals from PeV-A1 and PeV-A2 produced a strong, well-distributed green signal throughout the HT-29 cell layer, indicating robust early antigen replication and expression. PeV-A3 and PeV-A4 also showed good antigen positivity, while PeV-A5 and PeV-A6 showed weaker and more clustered green fluorescence, similar to that seen in HuTu80 cells. The uninfected HT-29 control showed only blue nuclear staining with no detectable green signal, confirming P5C4 specificity.

Table 4: Quantification of infected cells in HuTu80 and HT-29 cell lines using FIJI. Total cells (blue; DAPI) and infected cells (green) were counted for PeV-A1–A6, and infection rates (%) were calculated. All used genotypes infected both cell lines. Infection ranged from 41–75% in HuTu80 and 61–91% in HT-29 cells, with a slightly higher infection observed in HT-29.

	HuTu80			**HT-29 cell**		
PeV-A Types	Blue	Green	Infection (%)	Blue	Green	Infection (%)
A1	193	145	75	83	62	75
A2	244	140	57	116	84	72
A3	178	97	55	111	84	75
A4	144	94	65	94	86	91
A5	200	103	41	135	82	61
A6	189	82	43	69	59	86

The results (Table 4) showed that all PeV-A genotypes (A1–A6) infected both HuTu80 and HT-29 cell lines, and that differences in infection levels between genotypes and between the two cell types were observed. In HuTu80 cells, the total cell counts (DAPI/blue) ranged from 144 to 244 cells, while the number of antigen-positive cells (green) varied across the used genotype strains. The infection rates were observed to range from 41% to 75%, with the highest infection observed for PeV-A1 (75%), followed by PeV-A4 (65%). Lower infection rates were noted for PeV-A5 (41%) and PeV-A6 (43%), indicating reduced levels of detectable infection in these genotypes.

Likewise, in HT-29 cells, total cell numbers ranged from 69 to 135 cells, with many antigen-positive cells present. Also, the infection rates ranged from 61% to 91%, with PeV-A4 showing the highest infection level (91%). The representative PeV-A6 also showed a high infection rate (86%), while PeV-A5 presented the lowest infection among the HT-29 samples (61%).

5. Discussion

This study aimed to determine the susceptibility of HuTu80 cells to PeV-A types 1–6 and to visualize viral infection using different antibodies. In addition, the study aimed to compare parechovirus infection in HuTu80 against HT29 and VeroE6, which have been previously used in parechovirus cultivation. Viral infection in HuTu80 was assessed and confirmed using multiple techniques, including subjective observation of cytopathic effect (CPE), antibody detection by immunofluorescence staining, viral RNA quantification by RT-qPCR, and antibody binding affinity using ELISA. My findings demonstrate that HuTu80 cells support the cultivation of most tested PeV-A types (1–6), with infections successfully visualized using both monoclonal (mAb) and polyclonal (pAb) antibodies, and viral RNA quantified from HuTu80–PeV-A cell cultures. The results were comparable to HT29, but not VeroE6, which proved not useful in IFA due to high background fluorescence.

5.1 Effect of culture conditions for efficient PeV-A infection in HuTu80

The serum concentration in the medium and the selection of appropriate culture conditions are key for cell growth and reliable virus infectivity assays, especially when cytopathic effect is used as part of the assessment. It was observed that serum concentration had a clear impact on HuTu80 cell growth. Cells cultured in 10% FBS-EMEM showed good morphology, higher viability, and faster proliferation compared to those maintained in 5% FBS. This is in line with the established role of foetal bovine serum as a source of essential growth factors, hormones, and nutrients required for optimal cell survival and division (Park et al., 2026). As a result, low serum conditions can limit cell growth, proliferation, and metabolic activity, which may negatively affect viral replication and detection.

Moreover, for optimal CPE assessment, aside from considering serum concentration, it is essential to choose the ideal culture plate. Amongst the plates tested, Sarstedt plates seem to support the most uniform and well-dispersed HuTu80 cell monolayer, which is critical for consistent viral infection and accurate interpretation of CPE. Meanwhile, cells grown in Greiner and Corning plates exhibited edge-clustering. This effect may be due to differences in well hydrophilicity, surface treatment, and well geometry, which are key players in influencing cell attachment and distribution. Previous studies have shown that the surface properties of plate culture plastics significantly affect cell adhesion, spreading, and morphology, thereby impacting experimental outcomes (Curtis et al., 1983; Majhy et al., 2021). Accurate assessment

of CPE from PeV-A infection may be unclear due to inconsistencies arising from uneven cell distribution.

5.2 Dose-dependent cytopathic effects of PeV-A in HuTu80 Cells

To visualize viral infection and replication by monitoring PeV-A-induced morphological changes in HuTu80 cells, CPE-based testing was conducted. To confirm that observed cytopathic effects (CPE) were virus-specific and not an artifact of sample cytotoxicity, HuTu80 cells were infected with serial dilutions of PeV-A types 1–6.

Across all six parechovirus genotypes, infection of HuTu80 cells showed a clear dose-dependent effect on cytopathogenicity. At the highest inoculum (10 µL), the cell monolayer broke down quickly, with increasing cell rounding and detachment visible within 24 hours. This is in line with previous studies showing that some PeV genotypes can cause rapid and strong CPE in permissive epithelial cells when the viral load is high (Takagi et al., 2022; Westerhuis et al., 2013). When the inoculum was reduced to 1 µL, the effect was less severe. CPE was still visible but developed more slowly, suggesting a slower spread of infection across the cells. At 0.1 µL, only minor changes in cell morphology were seen, which agrees with earlier reports that lower viral input can lead to weaker or delayed CPE, especially for genotypes that already show mild effects (Baumgarte et al., 2008; Benschop et al., 2010).

However, significant strain-dependent differences in replication kinetics were also observed. Strains of PeV-A1, -3, and -4 induced rapid and pronounced CPE as early as 1-day post-infection (DPI), resulting in widespread cell damage by 2-3 DPI. In contrast, some strains of PeV-2, -5, and -6 exhibited delayed or minimal CPE, with detectable effects emerging only at late time points or remaining consistently weak across all replicates. This pattern within strains could represent intrinsic differences in cytopathogenicity. Some showed visible CPE even at lower inoculum levels, while others required higher viral input to produce similar changes. Those that did not show infectivity may be because they do not produce CPE particles, or the viral load is low. This suggests differences in how PeV types replicate and interact with cells, including variation in receptor use and replication speed (Al-Sunaidi et al., 2007; Seitsonen et al., 2010). The uninfected HuTu80 cells remained healthy and formed a normal, intact monolayer, confirming that the observed changes were due to viral infection.

These findings contrast with prior challenges in culturing newer PeV-A genotypes. Earlier studies identified the absence of a universal cell line, with HT-29 and Vero E6 being among the

few lines capable of supporting some PeV-A growth, but with low CPE induction, particularly for types like PeV-A3 and PeV-A6, which contributed to their delayed discovery. Inefficient propagation of PeV-A3 in HT-29 cells has been reported . The pronounced and distinct CPE observed here in PeV-A-infected HuTu80 cells suggests that HuTu80 cells may be more permissive to infection of a wider range of PeV-A types. Again, this follows previous findings and shows the value of using a consistent cell model, such as HuTu80, when comparing different HPeV types (Takagi et al., 2022).

The molecular basis for this susceptibility may be explained by the specific expression of the αVβ1 integrin receptor on HuTu80 cells. Research has established that PeV-A1 entry and replication depend strictly on αVβ1 and not on related integrins like αVβ3 or αVβ6 (Merilahti et al., 2016; Seitsonen et al., 2010). It is therefore possible that in HuTu80 cells, αVβ1 serves as the primary receptor for PeV-A1, facilitating entry via clathrin-dependent endocytosis, a mechanism that may extend to other PeV-A types.

5.3 Immunofluorescence analysis of PeV-A antigen expression in HuTu80 cells

Since all six PeV-A genotypes produced measurable cytopathic effects in HuTu80 cells, an immunofluorescence assay (IFA) was carried out to further confirm infection at the cellular level and to assess whether different antibody preparations could detect PeV-A viral antigen expression. While CPE provided an initial indication of infection, relying on subjective morphological changes alone can be limiting, especially for certain parechovirus genotypes. Previous studies have shown that genotypes such as PeV-A4, PeV-A5, and PeV-A6 often produce weak, delayed, or inconsistent cytopathic effects, making it difficult to consistently identify infection based on cell morphology alone (Al-Sunaidi et al., 2007; Baumgarte et al., 2008; Westerhuis et al., 2013). In some cases, infected cells may show only subtle intracellular changes without clear rounding or detachment, which further highlights the importance of using antibody-based methods to confirm infection and to compare antigen expression across different strains.

To address this, a panel of antibodies with different properties was used (Appendix 3). This included a monoclonal antibody P5C4, four polyclonal antibodies (PAb-K8873, K8851, K306, and K316), and three single-chain variable fragments (scFv-55, scFv-59, and scFv-71). Because crude polyclonal antibodies often contain components that can bind non-specifically to host cell structures, all polyclonal preparations were first purified using uninfected HuTu80 cells. This

step was important to reduce background staining and improve the clarity of the signal. Similar purification strategies have been recommended in studies involving epithelial cell lines, which express surface molecules such as integrins and adhesion proteins that can interact with unpurified antisera and lead to nonspecific binding (Curtis et al., 1983; Majhy et al., 2021). After purification, the overall signal-to-noise ratio improved, making it easier to distinguish true antigen staining from background fluorescence.

For assay validation, the dsRNA-specific monoclonal antibody J2 was used as a positive control. J2 is widely used to detect double-stranded RNA intermediates that are produced during viral replication, making it a reliable marker of active infection (Joki-Korpela & Hyypiä, 2001; Krogerus et al., 2003). In contrast, uninfected HuTu80 cells stained with each antibody preparation served as negative controls, allowing background fluorescence and nonspecific binding to be assessed. This combination of positive and negative controls helped to ensure that the observed staining patterns were specific to only viral infection.

Across all PeV-A genotypes, J2 produced strong and consistent cytoplasmic fluorescence, confirming that active viral replication was occurring in the PeV-A HuTu80-infected cells. This observation is in agreement with earlier studies showing that the accumulation of double-stranded RNA is a common feature of picornavirus replication complexes (Krogerus et al., 2003). In comparison with the fluorescence signal patterns observed with P5C4, the scFv antibodies did not produce a detectable staining signal in any of the genotypes tested. There is no explanation as to why this outcome, we assume maybe because the antibodies were too old or the antibodies were not compatible with the protocol used. Although these smaller antibody fragments are often expected to have better access to certain epitopes, their performance can be affected by reduced binding affinity or loss of conformational epitope recognition during recombinant expression and purification. Similar limitations have been reported in earlier studies (Tripathi et al., 2021). The lack of signal in this study suggests that the scFv antibodies were not suitable for detecting PeV-A viral antigens under the experimental conditions used.

Our result altogether shows varying antigen-detection patterns observed among PeV-A1 to PeV-A6, suggesting useful insight into how these viruses behave in epithelial cells during the early stages of infection. PeV-A1 to A3 each presented strong, diffuse antigen staining, which may play a role in efficient receptor engagement and quick establishment of replication complexes. This aligns with existing knowledge that these PeV-A types make efficient use of integrins such as αVβ1, αVβ3, and αVβ6 for cell entry (Joki-Korpela & Hyypiä, 2001; Merilahti

et al., 2016; Seitsonen et al., 2010). Also, recent work has identified MYADM as an important entry factor for PeV-A1 and PeV-A3, which further supports the high infectivity of these genotypes in epithelial cells (Qiao et al., 2024; Watanabe et al., 2023).

By contrast, PeV-A5 and A6 showed weaker intracellular fluorescence, which may likely suggest less efficient entry or slower replication. These differences probably came from variations in capsid structure and receptor usage, which have been shown to influence both antigen accessibility and replication efficiency (Al-Sunaidi et al., 2007; Shakeel et al., 2016; Tripathi et al., 2021). Additionally, these laboratory observations reflect real-world clinical patterns where PeV-A1 and PeV-A3 are frequently associated with symptomatic infections in infants, including sepsis-like illness and CNS involvement, whereas PeV-A4 through A6 tend to circulate more quietly in the community with variable pathogenicity (Esposito et al., 2014; Wang et al., 2020; Wolthers et al., 2008).

Thus, the IFA provided a sensitive and informative way to confirm infection and to examine antigen expression across PeV-A genotypes. Together, these results demonstrate the value of combining morphological, immunological, and molecular approaches to gain a more complete understanding of parechovirus infection.

5.4 RT-qPCR validation of CPE and IFA findings of PeV-A Replication in HuTu80 Cells

To further confirm the presence of viral infection, RT-qPCR was employed as an independent molecular assay to detect and quantify the viral RNA genomes of Parechovirus isolates (PeV-A1 to PeV-A6). The RT-qPCR analysis provided more molecular confirmation of the infection patterns observed through cytopathic effect (CPE) and immunofluorescence assays (IFA). The assay showed very good linearity, with R^2 values ranging from 0.99963 to 1.000 (Appendix 7). In real-time PCR, values close to 1 are generally taken as a sign that the standard curve is reliable and that the assay can quantify samples accurately across a wide range (Bustin et al., 2009). These high R^2 values suggest that there was very little variation between the dilution points.

The amplification efficiencies ranged from 82% to 99%, which are within or close to the acceptable range for diagnostic qPCR assays. Although efficiencies between 90% and 110% are generally considered optimal, slightly lower values can still be acceptable when the assay shows good linearity and consistent Ct values across serial dilutions (McLeish et al., 2012;

Taylor et al., 2010). The sensitivity observed in this study is consistent with earlier RT-qPCR assays developed for parechoviruses, which target conserved regions of the viral genome and can detect low levels of viral RNA, in the range of tens to a few hundred copies per reaction (Benschop et al., 2008; Nix et al., 2008).

PeV-A samples with low Ct values (~15–16) correspond to high viral loads (>10^6 copies/µL), while PeV-A samples with Ct ~28–29 show low copy numbers (~10^2–10^3 copies/µL). This pattern is biologically reasonable and reflects the variation in viral loads commonly seen in parechovirus infections. Similar trends have been reported in clinical studies, particularly in pediatric cases, where PeV-A3 is often linked to high levels of viremia during acute infection (Wolthers et al., 2008). All PeV-A1 to PeV-A6 isolates showed low Ct values (around 20) and high viral genome copy numbers compared to the controls, indicating strong viral replication in HuTu80 cells.

These results are in line with the phenotypic observations, where isolates such as PeV-A1, PeV-A3, and PeV-A4 produced clear CPE (Figure 6) and a high number of antigen-positive cells by IFA (Figure 8). The strong correlation between high viral RNA levels and strong CPE/IFA signals further supports that HuTu80 cells are permissive to multiple PeV-A genotypes, which agrees with previous studies (Baumgarte et al., 2008; Westerhuis et al., 2013). Studies have also reported differences in replication patterns between genotypes, especially for PeV-A3 and PeV-A6, which can result in more subtle or variable CPE (Esposito et al., 2014; Harvala et al., 2011). These differences in replication dynamics have been linked to factors such as receptor usage and replication efficiency in previous studies (Joki-Korpela & Hyypiä, 2001; Krogerus et al., 2003; Shakeel et al., 2016)

RT-qPCR was particularly useful for isolates that showed weaker CPE or lower fluorescence signals. For example, PeV-A5 and PeV-A6 produced less pronounced CPE and fewer antigen-positive cells, but RT-qPCR still detected high levels of viral RNA (Appendix 6). This confirms that these viruses were actively replicating despite presenting weaker phenotypic signals. Similar observations have been reported in previous studies, where some parechovirus genotypes show delayed or limited cytopathic effects (Al-Sunaidi et al., 2007; Drexler et al., 2009).

However, while many recent PeV-A isolates reacted with P5C4, the older 1994 samples (previously classified as Echovirus 22) did not. This is suggestive that these samples did not

contain detectable PeV-A RNA, which may be consistent with their known differences from modern PeV-A strains (Schnurr et al., 1996; Stanway et al., 1994). This highlights both the specificity of P5C4 and the importance of combining molecular and antibody-based methods for accurate virus identification (Abed et al., 2007; Harvala et al., 2010).

The RT-qPCR results also supported the IFA data obtained under the optimized conditions used in this study. The selected inoculum (10 µL) and P5C4 concentration (44 µg/mL) gave clear fluorescence signals with low background, and RT-qPCR confirmed that these conditions corresponded to high viral RNA levels. The consistency between molecular assay and antibody-based detection agrees with previous studies showing that real-time RT-PCR is highly sensitive and correlates well with viral replication (Bennett et al., 2011). RT-PCR is widely used for detecting parechovirus RNA, especially in cases where CPE is weak or absent (Benschop et al., 2008; Renaud et al., 2011).

The use of IVT RNA standards and no-template controls confirmed that the assay performed successfully. The IVT dilution series showed the expected increase in Ct values with decreasing RNA concentration, indicating good linearity, while the absence of amplification in NTCs confirmed that there was no contamination. Similar results have been reported in earlier studies on enteroviruses and parechoviruses (McLeish et al., 2012; Österback et al., 2013).

Finally, the combined CPE, IFA, and RT-qPCR results highlight clear differences in how the different PeV-A genotypes replicate and express viral proteins. Genotypes such as PeV-A3 and PeV-A4 showed strong CPE, high antigen expression, and high RNA levels, indicating efficient replication. In contrast, PeV-A6 showed weaker CPE and lower antigen detection, but still produced measurable viral RNA, suggesting ongoing replication at a lower level or with reduced antigen visibility. Using both molecular and phenotypic methods is important when studying human parechoviruses, since different genotypes can show varying patterns of infection and replication (Wang et al., 2020; Wolthers et al., 2008).

5.5 Correlation of ELISA with CPE, IFA, and RT-qPCR results

The ELISA results add a useful quantitative perspective to the findings from the CPE, IFA, and RT-qPCR experiments. Note, the CPE results showed that all six PeV-A genotypes were able to infect HuTu80 cells, but the extent of visible cell damage varies across all isolates. This was very obvious for PeV-A4 to A6, which are known to produce weaker or less consistent CPE in cell culture (Baumgarte et al., 2008; Westerhuis et al., 2013). Thus, relying on cell morphology

alone can sometimes underestimate viral infection. The ELISA helps overcome this by directly measuring antigen–antibody binding, making it easier to detect the presence of a virus even when visible changes in cells are limited.

As earlier reported, the IFA results also showed clear differences between PeV-A genotypes. PeV-A1 to A3 produced stronger fluorescence signals compared to PeV-A5 and A6, which showed weaker and more localized staining. However, because IFA is not fully quantitative and can be affected by many factors such as antibody binding strength, viral epitope availability, and background signal, it can be difficult to tell if weaker staining reflects lower antigen levels or only low antibody recognition. The ELISA results help to clarify this. The increase in absorbance with higher antibody concentration, and the observed stronger signal at 5 µg/ml compared to 2.5 µg/ml, show that P5C4 successfully binds viral antigens across the different PeV-A genotypes tested. The differences in absorbance between isolates follow the same trend seen in IFA, suggesting that the weaker signals in PeV-A5 and A6 are more likely due to real differences in antigen presentation rather than technical limitations.

The RT-qPCR data also support these findings by confirming that all six genotypes replicated in HuTu80 cells, even in cases where CPE or IFA signals were less obvious. This is in line with earlier reports showing that some parechovirus genotypes can replicate without producing strong CPE, especially those with differences in capsid structure or receptor usage (Al-Sunaidi et al., 2007; Shakeel et al., 2016). The ELISA results validate this by showing that PeV-A viral proteins are not only replicated but are also detectable by antibody binding, which supports the idea that infection was successful across all used PeV-A isolates.

This means ELISA acts as a link between the visual observations from CPE and IFA and the molecular data from RT-qPCR. This highlights the importance of using a combination of methods when studying parechoviruses, especially because of the differences in how each genotype behaves in culture medium.

5.6 Comparative PeV-A infection efficiency and immunofluorescence performance in HuTu80, HT-29, and VeroE6 cell lines

The quantitative image analysis of HuTu80 and HT-29 cells provided an extra dimension to the previous CPE, IFA, and RT-qPCR findings. It also helps to explain how well each cell line supports replication of PeV-A1 to A6 under the conditions used. The six PeV-A genotypes were

able to infect both HuTu80 and HT-29, but there were differences in the infection rates observed between genotypes and between the two intestinal cell lines.

These findings align well with previous studies about PeV-A growth characteristics in different cell lines. Westerhuis et al. (2013) compared PeV-A1 to A6 replication on multiple cell lines and showed that the viral growth is very cell-type dependent, stating that the human intestinal cell lines support more pronounced viral replication than non-intestinal lines. The study further stated that some PeV-A genotypes replicate efficiently in one cell line but poorly in others, thus reflecting differences in receptor protein expression, intracellular environment, and innate immune responses (Westerhuis et al., 2013). Our observation that HT-29 tends to yield higher infection rates than HuTu80 for most genotypes is therefore in tandem with the notion that similarly related intestinal lines can differ in how permissive they can be to PeV-A replication.

As discussed in section 5.3, recent studies on host-cell factors provide a crucial explanation for the differences between HuTu80 and HT-29 cell lines. For example, Qiao et al. (2024) showed that MYADM binds to PeV-A1 and is used for viral entry, showing that this host receptor is a big determinant of susceptibility. In their study, they state the importance of MYADM binding to human parechovirus-1, which is an essential mechanism for viral entry, thus linking a specific host protein to successful viral infection (Qiao et al., 2024). Another study showed that MYADM is also essential for PeV-A3 entry, suggesting that MYADM is a shared entry factor for multiple PeV-A genotypes (Watanabe et al., 2023).

Takagi et al. (2022) recently identified a human intestinal cell line that is permissive for the propagation of human parechovirus type 1 to 6, the basis of our study, stating how PeV-A replication depends on the presence of appropriate human intestinal entry factors and a conducive cellular environment. Therefore, it is safe to infer that differences in MYADM expression or localization between HuTu80 and HT-29 could contribute to the higher infection rates observed in HT-29, even though both lines are of intestinal origin.

The poor performance of VeroE6 in the IFA experiments was clearly different from the quantifiable signals observed in HuTu80 and HT-29 cells. In VeroE6, the images showed high background, blurred fields, and in some cases, it was difficult to distinguish nuclei or GFP signal. Because of these limitations, infection was not quantified in this cell line. Hence, the results suggest that VeroE6 is not suitable for PeV-A detection using the IFA protocol applied in this study.

This observation is in line with previous knowledge about PeV-A cell tropism. Vero-derived cells originate from African green monkey kidney and do not represent the human intestinal environment, a natural target for parechoviruses (Joki-Korpela & Hyypiä, 2001; Stanway et al., 1994). These cells are also unlikely to express key human entry factors, such as MYADM, at appropriate levels, and this may limit viral entry and early antigen expression (Qiao et al., 2024; Watanabe et al., 2023). In addition, Vero cells are known to be sensitive to fixation and permeabilization, which can affect nuclear integrity and increase background fluorescence (Shaver et al., 1958; Wigand & Sabin, 1961). These factors likely explain the poor image quality observed, even if some level of viral replication may still have occurred.

Meanwhile, HuTu80 and HT-29 cells supported viral replication, as shown by CPE, clear IFA images, and RT-qPCR. This supports the growing view that human intestinal cell lines are more appropriate models for studying PeV-A, due to their relevance in gastrointestinal infections affecting infants and young children (Esposito et al., 2014; Harvala et al., 2010; Wolthers et al., 2008). In this study, both HuTu80 and HT-29 proved to be suitable for cultivating PeV-A 1-6, with HT-29 showing high infection rates and strong antigen detection with P5C4.

Overall, the results highlight that infection efficiency and detection depend strongly on the choice of cell line, including factors such as receptor expression, integrin usage, and compatibility with immunofluorescence methods (Merilahti et al., 2016; Seitsonen et al., 2010; Takagi et al., 2022). This study supports the use of appropriate human cell models when studying PeV-A infection and antigen detection.

5.7 Limitations of the study

Although this study provides useful insights into how PeV-A1 to PeV-A6 infect HuTu80 cells, a few limitations are worth noting. First, due to the number of isolates I used, there were no genotype-specific controls. Also, it is not certain that antibodies work in native cells or tissues.

Secondly, while the antibody panel was diverse, it did not include genotype-specific monoclonal antibodies for every PeV-A type to be used as controls. The antibodies used were also in-house antibodies developed by the lab, and there were little or no previous studies of antibody detection of PeV-A.

The lack of reactivity seen with the recombinant scFv antibodies also suggests that further optimisation or different antibody formats may be needed to properly characterise antigenic

differences between these PeV-A types. Finally, the quality of the virus samples was not known before the study, and I have addressed these issues with CPE.

5.8 Conclusion

The results from the CPE, IFA, RT-qPCR, and ELISA experiments show that PeV-A1 to A6 infect HuTu80 cells successfully. The CPE results gave the first indication of infection, while the IFA confirmed the presence of viral antigen inside the cells, via observable variation in staining intensity across genotypes. RT-qPCR further supported these findings by confirming active viral replication in all isolates used, even in cases where the visible effects were less pronounced.

Both HuTu80 and HT-29 cells supported productive infection by all six PeV-A genotypes, although clear differences were observed in how efficiently infection could be detected between the two cell lines. HuTu80 showed consistent viral replication, with some genotype-specific variation in antigen expression. In contrast, HT-29 showed higher overall infection rates and produced stronger and more uniform P5C4-mediated signals, making antigen detection more straightforward and reliable.

In comparison, VeroE6 did not produce interpretable IFA images, mainly due to high background and poor signal clarity. This shows its limited compatibility with antibody-based detection methods in this study and further supports the use of human intestinal cell models for visualizing PeV-A infection. The ELISA results added an important quantitative dimension by showing that the P5C4 antibody could detect viral antigens across the six PeV-A types. Meanwhile, it highlighted some differences in antigen levels and how easily these antigens could be recognised by the P5C4.

Summarily, these findings add to the current understanding of PeV-A cell tropism and provide a solid experimental basis for future studies investigating parechoviral entry, antigenicity, and host-virus interactions in cell models that support parechovirus infection.

Acknowledgements

My gratitude goes to my thesis supervisor, Dr. Petri Susi, for his immense support, guidance, encouragement, and training throughout the course of this thesis. I truly appreciate the opportunity to learn directly from him, as well as his prompt and constructive feedback, which played an important role in shaping this work and developing my scientific thinking and writing skills.

I am also thankful to members of his research group, especially Iines Auravuo, who was always willing to assist me with reviewing my protocols. I also appreciate my fellow master's colleagues, Tira Grahn, Esrat Jahan, and Lotta Putkiranta, for their support whenever I needed help. I would also like to acknowledge the entire staff at Medisiina D, 7th floor, Institute of Biomedicine, University of Turku, for their assistance, helpful discussions, and supportive working environment. I truly appreciate their willingness to share knowledge and provide technical support, which contributed to the successful completion of this project.

I would like to extend my appreciation to all staff of the Biomedical Imaging Master's Programme for the teaching and training that provided a valuable foundation for my academic and career development. I would especially like to thank Associate Professor Diana Toivola and Kari Vienola for their mentorship and guidance, which greatly contributed to my academic success.

Finally, I am very grateful to my family and friends for their unwavering support, understanding, and encouragement throughout my studies. Most especially, my husband, Mr. Ejike Aniefuna, for being my support system - both emotionally and financially. I overcame every challenge because you believed in me.

References

Abed, Y., Wolf, D., Dagan, R., & Boivin, G. (2007). Development of a Serological Assay Based on a Synthetic Peptide Selected from the VP0 Capsid Protein for Detection of Human Parechoviruses. *Journal of Clinical Microbiology*, *45*(6), 2037–2039. https://doi.org/10.1128/jcm.02432-06

Alam, F., Li, Y., & Vogt, M. R. (2025). Parechovirus: Neglected for too long? *Journal of Virology*, *99*(4), e0184624. https://doi.org/10.1128/jvi.01846-24

Alam, M. M., Khurshid, A., Shaukat, S., Rana, M. S., Sharif, S., Angez, M., Nisar, N., Naeem, M., & Zaidi, S. S. Z. (2013). Human Parechovirus Genotypes -10, -13 and -15 in Pakistani Children with Acute Dehydrating Gastroenteritis. *PLOS ONE*, *8*(11), e78377. https://doi.org/10.1371/journal.pone.0078377

Alho, A., Marttila, J., Ilonen, J., & Hyypiä, T. (2003). Diagnostic Potential of Parechovirus Capsid Proteins. *Journal of Clinical Microbiology*, *41*(6), 2294–2299. https://doi.org/10.1128/JCM.41.6.2294-2299.2003

Alshammari, A., Alotaibi, J., Almaghrabi, R., Bawazeer, R., Althawadi, S., & Tayeb, H. (2024). First parechovirus reported case in Saudi Arabia in hospitalized immunocompromised adult patient. *Virology Journal*, *21*(1), 102. https://doi.org/10.1186/s12985-024-02372-4

Al-Sunaidi, M., Williams, Ç. H., Hughes, P. J., Schnurr, D. P., & Stanway, G. (2007). Analysis of a New Human Parechovirus Allows the Definition of Parechovirus Types and the Identification of RNA Structural Domains. *Journal of Virology*, *81*(2), 1013–1021. https://doi.org/10.1128/JVI.00584-06

Andino, R., Kirkegaard, K., Macadam, A., Racaniello, V. R., & Rosenfeld, A. B. (2023). The Picornaviridae Family: Knowledge Gaps, Animal Models, Countermeasures, and

Prototype Pathogens. *The Journal of Infectious Diseases*, *228*(Suppl 6), S427–S445. https://doi.org/10.1093/infdis/jiac426

Baumgarte, S., de Souza Luna, L. K., Grywna, K., Panning, M., Drexler, J. F., Karsten, C., Huppertz, H. I., & Drosten, C. (2008). Prevalence, Types, and RNA Concentrations of Human Parechoviruses, Including a Sixth Parechovirus Type, in Stool Samples from Patients with Acute Enteritis. *Journal of Clinical Microbiology*, *46*(1), 242–248. https://doi.org/10.1128/jcm.01468-07

Bennett, S., Harvala, H., Witteveldt, J., McWilliam Leitch, E. C., McLeish, N., Templeton, K., Gunson, R., Carman, W. F., & Simmonds, P. (2011). Rapid Simultaneous Detection of Enterovirus and Parechovirus RNAs in Clinical Samples by One-Step Real-Time Reverse Transcription-PCR Assay. *Journal of Clinical Microbiology*, *49*(7), 2620–2624. https://doi.org/10.1128/jcm.02445-10

Benschop, K., Minnaar, R., Koen, G., van Eijk, H., Dijkman, K., Westerhuis, B., Molenkamp, R., & Wolthers, K. (2010). Detection of human enterovirus and human parechovirus (HPeV) genotypes from clinical stool samples: Polymerase chain reaction and direct molecular typing, culture characteristics, and serotyping. *Diagnostic Microbiology and Infectious Disease*, *68*(2), 166–173. https://doi.org/10.1016/j.diagmicrobio.2010.05.016

Benschop, K., Molenkamp, R., van der Ham, A., Wolthers, K., & Beld, M. (2008). Rapid detection of human parechoviruses in clinical samples by real-time PCR. *Journal of Clinical Virology*, *41*(2), 69–74. https://doi.org/10.1016/j.jcv.2007.10.004

Benschop, K., Thomas, X., Serpenti, C., Molenkamp, R., & Wolthers, K. (2008). High prevalence of human Parechovirus (HPeV) genotypes in the Amsterdam region and identification of specific HPeV variants by direct genotyping of stool samples. *Journal of Clinical Microbiology*, *46*(12), 3965–3970. https://doi.org/10.1128/JCM.01379-08

Britton, P. N., Khandaker, G., Khatami, A., Teutsch, S., Francis, S., McMullan, B. J., & Jones, C. A. (2018). High prevalence of developmental concern amongst infants at 12 months following hospitalised parechovirus infection. *Journal of Paediatrics and Child Health*, *54*(3), 289–295. https://doi.org/10.1111/jpc.13728

Brouwer, L., Wolthers, K. C., & Pajkrt, D. (2020). Parechovirus A prevalence in adults in The Netherlands. *Archives of Virology*, *165*(4), 963–966. https://doi.org/10.1007/s00705-020-04547-0

Bustin, S. A., Benes, V., Garson, J. A., Hellemans, J., Huggett, J., Kubista, M., Mueller, R., Nolan, T., Pfaffl, M. W., Shipley, G. L., Vandesompele, J., & Wittwer, C. T. (2009). The MIQE guidelines: Minimum information for publication of quantitative real-time PCR experiments. *Clinical Chemistry*, *55*(4), 611–622. https://doi.org/10.1373/clinchem.2008.112797

Curtis, A. S., Forrester, J. V., McInnes, C., & Lawrie, F. (1983). Adhesion of cells to polystyrene surfaces. *The Journal of Cell Biology*, *97*(5 Pt 1), 1500–1506. https://doi.org/10.1083/jcb.97.5.1500

Drexler, J. F., Grywna, K., Stöcker, A., Almeida, P. S., Ribeiro, T. C. M., Eschbach-Bludau, M., Petersen, N., Ribeiro, H. da C., & Drosten, C. (2009). Novel Human Parechovirus from Brazil. *Emerging Infectious Diseases*, *15*(2), 310–313. https://doi.org/10.3201/eid1502.081028

Esposito, S., Rahamat-Langendoen, J., Ascolese, B., Senatore, L., Castellazzi, L., & Niesters, H. G. M. (2014). Pediatric parechovirus infections. *Journal of Clinical Virology*, *60*(2), 84–89. https://doi.org/10.1016/j.jcv.2014.03.003

Ghazi, F., Hughes, P. J., Hyypiä, T., & Stanway, G. (1998). Molecular analysis of human parechovirus type 2 (formerly echovirus 23). *The Journal of General Virology*, *79 (Pt 11)*, 2641–2650. https://doi.org/10.1099/0022-1317-79-11-2641

Harvala, H., McLeish, N., Kondracka, J., McIntyre, C. L., McWilliam Leitch, E. C., Templeton, K., & Simmonds, P. (2011). Comparison of human parechovirus and enterovirus detection frequencies in cerebrospinal fluid samples collected over a 5-year period in edinburgh: HPeV type 3 identified as the most common picornavirus type. *Journal of Medical Virology*, *83*(5), 889–896. https://doi.org/10.1002/jmv.22023

Harvala, H., Wolthers, K. C., & Simmonds, P. (2010). Parechoviruses in children: Understanding a new infection. *Current Opinion in Infectious Diseases*, *23*(3), 224–230. https://doi.org/10.1097/qco.0b013e32833890ca

Ito, M., Yamashita, T., Tsuzuki, H., Kabashima, Y., Hasegawa, A., Nagaya, S., Kawaguchi, M., Kobayashi, S., Fujiura, A., Sakae, K., & Minagawa, H. (2010). Detection of human parechoviruses from clinical stool samples in Aichi, Japan. *Journal of Clinical Microbiology*, *48*(8), 2683–2688. https://doi.org/10.1128/JCM.00086-10

Ito, M., Yamashita, T., Tsuzuki, H., Takeda, N., & Sakae, K. (2004). Isolation and identification of a novel human parechovirus. *The Journal of General Virology*, *85*(Pt 2), 391–398. https://doi.org/10.1099/vir.0.19456-0

Joki-Korpela, P., Marjomäki, V., Krogerus, C., Heino, J., & Hyypiä, T. (2001). Entry of Human Parechovirus 1. *Journal of Virology*, *75*(4), 1958–1967. https://doi.org/10.1128/jvi.75.4.1958-1967.2001

Joki-Korpela, P., Roivainen, M., Lankinen, H., Pöyry, T., & Hyypiä, T. (2000). Antigenic properties of human parechovirus 1. *The Journal of General Virology*, *81*(Pt 7), 1709–1718. https://doi.org/10.1099/0022-1317-81-7-1709

Joki-Korpela, Päi., & Hyypiä, T. (2001). Parechoviruses, a novel group of human picornaviruses. *Annals of Medicine*, *33*(7), 466–471. https://doi.org/10.3109/07853890109002095

King, A. M. Q., Lefkowitz, E. J., Mushegian, A. R., Adams, M. J., Dutilh, B. E., Gorbalenya, A. E., Harrach, B., Harrison, R. L., Junglen, S., Knowles, N. J., Kropinski, A. M., Krupovic, M., Kuhn, J. H., Nibert, M. L., Rubino, L., Sabanadzovic, S., Sanfaçon, H., Siddell, S. G., Simmonds, P., … Davison, A. J. (2018). Changes to taxonomy and the International Code of Virus Classification and Nomenclature ratified by the International Committee on Taxonomy of Viruses (2018). *Archives of Virology*, *163*(9), 2601–2631. https://doi.org/10.1007/s00705-018-3847-1

Kolehmainen, P., Oikarinen, S., Koskiniemi, M., Simell, O., Ilonen, J., Knip, M., Hyöty, H., & Tauriainen, S. (2012). Human parechoviruses are frequently detected in stool of healthy Finnish children. *Journal of Clinical Virology*, *54*(2), 156–161. https://doi.org/10.1016/j.jcv.2012.02.006

Krogerus, C., Egger, D., Samuilova, O., Hyypiä, T., & Bienz, K. (2003). Replication Complex of Human Parechovirus 1. *Journal of Virology*, *77*(15), 8512–8523. https://doi.org/10.1128/jvi.77.15.8512-8523.2003

Majhy, B., Priyadarshini, P., & Sen, A. K. (n.d.). Effect of surface energy and roughness on cell adhesion and growth – facile surface modification for enhanced cell culture. *RSC Advances*, *11*(25), 15467–15476. https://doi.org/10.1039/d1ra02402g

Majhy, B., Priyadarshini, P., & Sen, A. K. (2021). Effect of surface energy and roughness on cell adhesion and growth—Facile surface modification for enhanced cell culture. *RSC Advances*, *11*(25), 15467–15476. https://doi.org/10.1039/d1ra02402g

McLeish, N. J., Witteveldt, J., Clasper, L., McIntyre, C., McWilliam Leitch, E. C., Hardie, A., Bennett, S., Gunson, R., Carman, W. F., Feeney, S. A., Coyle, P. V., Vipond, B., Muir, P., Benschop, K., Wolthers, K., Waris, M., Osterback, R., Johannessen, I., Templeton, K., Simmonds, P. (2012). Development and Assay of RNA Transcripts of Enterovirus Species A to D, Rhinovirus Species A to C, and Human Parechovirus: Assessment of

Assay Sensitivity and Specificity of Real-Time Screening and Typing Methods. *Journal of Clinical Microbiology*, *50*(9), 2910–2917. https://doi.org/10.1128/jcm.01172-12

Merilahti, P., Tauriainen, S., & Susi, P. (2016). Human Parechovirus 1 Infection Occurs via αVβ1 Integrin. *PLOS ONE*, *11*(4), e0154769. https://doi.org/10.1371/journal.pone.0154769

Minor, P. D., Ferguson, M., Evans, D. M., Almond, J. W., & Icenogle, J. P. (1986). Antigenic structure of polioviruses of serotypes 1, 2 and 3. *The Journal of General Virology*, *67 (Pt 7)*, 1283–1291. https://doi.org/10.1099/0022-1317-67-7-1283

Nix, W. A., Maher, K., Johansson, E. S., Niklasson, B., Lindberg, A. M., Pallansch, M. A., & Oberste, M. S. (2008). Detection of All Known Parechoviruses by Real-Time PCR. *Journal of Clinical Microbiology*, *46*(8), 2519–2524. https://doi.org/10.1128/JCM.00277-08

Österback, R., Tevaluoto, T., Ylinen, T., Peltola, V., Susi, P., Hyypiä, T., & Waris, M. (2013). Simultaneous Detection and Differentiation of Human Rhino- and Enteroviruses in Clinical Specimens by Real-Time PCR with Locked Nucleic Acid Probes. *Journal of Clinical Microbiology*, *51*(12), 3960–3967. https://doi.org/10.1128/JCM.01646-13

Padala, S. A., & Kallam, A. (2025). Diffuse Large B-Cell Lymphoma. In *StatPearls*. StatPearls Publishing. http://www.ncbi.nlm.nih.gov/books/NBK557796/

Park, J., Lee, D.-Y., Mariano, E. J., Choi, Y., Han, D., Kim, J. S., Park, J. W., Namkung, S., Lee, S. Y., Lee, H. W., Lee, H. J., & Hur, S. J. (2026). Review of culture media and serum substitutes containing phytoecdysteroids for application in cultured meat technology. *Food Science of Animal Resources*, *46*(1), 1. https://doi.org/10.1007/s44463-025-00003-2

Qiao, W., Richards, C. M., Kim, Y., Zengel, J. R., Ding, S., Greenberg, H. B., & Carette, J. E. (2024). MYADM binds human parechovirus 1 and is essential for viral entry. *Nature Communications*, *15*(1), 3469. https://doi.org/10.1038/s41467-024-47825-0

Renaud, C., Kuypers, J., Ficken, E., Cent, A., Corey, L., & Englund, J. A. (2011). Introduction of a novel parechovirus RT-PCR clinical test in a regional medical center. *Journal of Clinical Virology*, *51*(1), 50–53. https://doi.org/10.1016/j.jcv.2011.02.010

Schnurr, D., Dondero, M., Holland, D., & Connor, J. (1996). Characterization of echovirus 22 variants. *Archives of Virology*, *141*(9), 1749–1758. https://doi.org/10.1007/BF01718297

Seitsonen, J., Susi, P., Heikkilä, O., Sinkovits, R. S., Laurinmäki, P., Hyypiä, T., & Butcher, S. J. (2010). Interaction of αVβ3 and αVβ6 Integrins with Human Parechovirus 1. *Journal of Virology*, *84*(17), 8509–8519. https://doi.org/10.1128/JVI.02176-09

Shakeel, S., Westerhuis, B. M., Domanska, A., Koning, R. I., Matadeen, R., Koster, A. J., Bakker, A. Q., Beaumont, T., Wolthers, K. C., & Butcher, S. J. (2016). Multiple capsid-stabilizing interactions revealed in a high-resolution structure of an emerging picornavirus causing neonatal sepsis. *Nature Communications*, *7*, 11387. https://doi.org/10.1038/ncomms11387

Shaver, D. N., Barron, A. L., & Karzon, D. T. (1958). Cytopathology of Human Enteric Viruses in Tissue Culture. *The American Journal of Pathology*, *34*(5), 943–963. https://pmc.ncbi.nlm.nih.gov/articles/PMC1934761/

Sridhar, A., Karelehto, E., Brouwer, L., Pajkrt, D., & Wolthers, K. C. (2019). Parechovirus A Pathogenesis and the Enigma of Genotype A-3. *Viruses*, *11*(11), 1062. https://doi.org/10.3390/v11111062

Stanway, G., & Hyypiä, T. (1999). Parechoviruses. *Journal of Virology*. (world). https://doi.org/10.1128/jvi.73.7.5249-5254.1999

Stanway, G., Kalkkinen, N., Roivainen, M., Ghazi, F., Khan, M., Smyth, M., Meurman, O., & Hyypiä, T. (1994). Molecular and biological characteristics of echovirus 22, a representative of a new picornavirus group. *Journal of Virology*, *68*(12), 8232–8238. https://doi.org/10.1128/jvi.68.12.8232-8238.1994

Takagi, H., Oka, T., Ami, Y., Suzaki, Y., & Saito, H. (2022). A Human Intestinal Cell Line Suitable for the Propagation of Human Parechovirus Type 1 to 6 with a Clear Cytopathic Effect. *Japanese Journal of Infectious Diseases*, *75*(3), 318–321. https://doi.org/10.7883/yoken.JJID.2021.534

Taylor, S., Wakem, M., Dijkman, G., Alsarraj, M., & Nguyen, M. (2010). A practical approach to RT-qPCR—Publishing data that conform to the MIQE guidelines. *Methods, The Ongoing Evolution of qPCR*, *50*(4), S1–S5. https://doi.org/10.1016/j.ymeth.2010.01.005

Tripathi, L., Hietanen, E., Merilahti, P., Teixido, L., Sanchez-Alberola, N., Tauriainen, S., & Susi, P. (2021a). Monoclonal antibody against VP0 recognizes a broad range of human parechoviruses. *Journal of Virological Methods*, *293*, 114167. https://doi.org/10.1016/j.jviromet.2021.114167

Tripathi, L., Hietanen, E., Merilahti, P., Teixido, L., Sanchez-Alberola, N., Tauriainen, S., & Susi, P. (2021b). Monoclonal antibody against VP0 recognizes a broad range of human parechoviruses. *Journal of Virological Methods*, *293*, 114167. https://doi.org/10.1016/j.jviromet.2021.114167

Verboon-Maciolek, M. A., Groenendaal, F., Hahn, C. D., Hellmann, J., van Loon, A. M., Boivin, G., & de Vries, L. S. (2008). Human parechovirus causes encephalitis with white matter injury in neonates. *Annals of Neurology*, *64*(3), 266–273. https://doi.org/10.1002/ana.21445

Walls, T. (2017). Human Parechovirus: An Increasingly Recognized Cause of Sepsis-Like Illness in Young Infants. *Clinical Microbiology Reviews*, *31*. https://doi.org/10.1128/CMR.00047-17

Wang, C. Y. T., Ware, R. S., Lambert, S. B., Mhango, L. P., Tozer, S., Day, R., Grimwood, K., & Bialasiewicz, S. (2020). Parechovirus A Infections in Healthy Australian Children During the First 2 Years of Life: A Community-based Longitudinal Birth Cohort Study. *Clinical Infectious Diseases*, *71*(1), 116–127. https://doi.org/10.1093/cid/ciz761

Watanabe, K., Oka, T., Takagi, H., Anisimov, S., Yamashita, S., Katsuragi, Y., Takahashi, M., Higuchi, M., Kanki, T., Saitoh, A., & Fujii, M. (2023). Myeloid-associated differentiation marker is an essential host factor for human parechovirus PeV-A3 entry. *Nature Communications*, *14*(1), 1817. https://doi.org/10.1038/s41467-023-37399-8

Westerhuis, B. M., Jonker, S. C., Mattao, S., Benschop, K. S., & Wolthers, K. C. (2013). Growth characteristics of human parechovirus 1 to 6 on different cell lines and cross-neutralization of human parechovirus antibodies: A comparison of the cytopathic effect and real time PCR. *Virology Journal*, *10*, 146. https://doi.org/10.1186/1743-422X-10-146

Wigand, R., & Sabin, A. B. (1961). Properties of ECHO types 22, 23 and 24 viruses. *Archiv Für Die Gesamte Virusforschung*, *11*(2), 224–247. https://doi.org/10.1007/BF01241688

Wildenbeest, J. G., Benschop, K. S. M., Bouma-de Jongh, S., Wolthers, K. C., & Pajkrt, D. (2016). Prolonged Shedding of Human Parechovirus in Feces of Young Children after Symptomatic Infection. *The Pediatric Infectious Disease Journal*, *35*(5), 580. https://doi.org/10.1097/INF.0000000000001082

Wolthers, K. C., Benschop, K. S. M., Schinkel, J., Molenkamp, R., Bergevoet, R. M., Spijkerman, I. J. B., Kraakman, H. C., & Pajkrt, D. (2008). Human Parechoviruses as an Important Viral Cause of Sepsislike Illness and Meningitis in Young Children. *Clinical Infectious Diseases*, *47*(3), 358–363. https://doi.org/10.1086/589752

Zell, R., Knowles, N. J., & Simmonds, P. (2021). A proposed division of the family Picornaviridae into subfamilies based on phylogenetic relationships and functional genomic organization. *Archives of Virology*, *166*(10), 2927–2935. https://doi.org/10.1007/s00705-021-05178-9

Appendices

Appendix 1: PeV-A strains used in preliminary infection experiments with HuTu80 Cells.

Types	Strains	Types	Strains
PeV-A1	Harris	PeV-1	50112 04759
PeV-A3	145-8	PeV-1	50687 04768
PeV-A1	153-20	PeV-1	50177 04432
PeV-A1	150-8	PeV-1	50504 04763
PeV-A1	145-12	PeV-1	50581 04764
PeV-A1	125-7	PeV-3	A308/99
PeV-A1	103-2	PeV-3	88
PeV-A2	Williamson	PeV-3	K251181-02
PeV-A2	Williamson (1964 HeLa)	PeV-3	145(8)
PeV-A4	FI121236	PeV-3	K251181-02
PeV-A3	88	PeV-3	K251181-02
PeV-A4	20152401	PeV-3	3 (252277)
PeV-A6	89	PeV-3	4 (252277)
PeV-A5	20552323	PeV-2	Williamson
PeV-A6	21152464	PeV-2	Williamson
PeV-A5	20552322	PeV-6	2005-823
PeV-A4	K251176	PeV-6	47
PeV-A3	252277	PeV-5	20552325
PeV-A3	152037	PeV-4	K251176
PeV-A3	K251181-02	PeV-2	Williamson

Appendix 2: PeV-A isolates used for IFA

PeV Type	Isolate
PeV-A1	Harris
PeV-A1	145-12
PeV-A2	Williamson
PeV-A3	152037
PeV-A3	A308/99
PeV-A3	K251181-02
PeV-A4	110402
PeV-A4	20152401
PeV-A5	20552322
PeV-A6	21152464

Appendix 3: Panel of primary antibodies used in the IFA.

Primary Antibodies	**Source**	**Primary Antibodies**	**Source**
P5C4 (mab)	mouse	purified Pab-K8851	rabbit
Pab-K8873	rabbit	purified Pab-K306	rabbit
Pab-K8851	rabbit	purified Pab-K316	rabbit
Pab-K306	rabbit	scFv-55	rabbit
Pab-K316	rabbit	scFv-59	rabbit
purified Pab-K8873	rabbit	scFv-71	rabbit

Appendix 4: Other PeV-A samples tested positive with P5C4 antibody via IFA

PeV type	Strain	P5C4	PeV Types	Strain	P5C4
PeV-A1	HarrisHarris	+	PeV-A6	21152464	+
PeV-A1	350757	+	PeV-A1	101-17	+
PeV-A1	152478	+	PeV-A1	125-7	+
PeV-A1	452252	+	PeV-A1	NIH Harris	-
PeV-A1	550163	+	PeV-A1	ATCC (Harris)	-
PeV-A1	153231	+	PeV-A1	Williamson	-
PeV-A1	19	+	PeV-A1	50024 04133	-
PeV-A1	80	+	PeV-A1	50112 04759	-
PeV-A1	83	+	PeV-A1	50687 04768	-
ECHO 22	Harris ATCC	-	PeV-A1	50177 04432	-

ECHO 22	Harris	-	PeV-A1	50504 04763	-
ECHO 22	89V-1385	+	PeV-A1	50581 04764	-
PeV-A2	Williamson	+	PeV-A1	50175 04322	-
PeV-A3	251360	+	PeV-A1	52284 04011	-
PeV-A3	73	+	PeV-A1	52486 04267	-
PeV-A3	88	+	PeV-A1	50077 04431	-
PeV-A3	I7=4/252277	+	PeV-A1	52883 04283	-
PeV-A3	E6 = 152037	+	PeV-A1	53618 04346	-
PeV-A3	E6 = 152037	+	PeV-A1	52980 04286	-
PeV-A3	FI0688	+	PeV-A1	52590 04274	-
PeV-A6	47	+	PeV-A1	54003 04026	-
PeV-A1	452252	+	PeV-A1	53657 04024	-
PeV-A1	350757	+	PeV-A1	56863 04380	-
PeV-A1	550163	+	PeV-A1	50116 04197	-
PeV-A1	153231	+	PeV-A1	50498 04325	-
PeV-A4	K251176-02	+	PeV-A1	50489 04001	-
PeV-A5	20552325	+	PeV-A1	50077 04753	-

Appendix 5: PeV isolates used for ELISA & RT-qPCR

PeV Type	Isolates		PeV Type	Isolates
PeV-1	Harris		PeV-3	152037
PeV-1	150-8		PeV-3	K251181-02
PeV-1	145-12		PeV-3	A308/99
PeV-1	103-2		PeV-3	K251181-02
PeV-4	110402		PeV-3	K251181-02
PeV-4	20152401		PeV-2	
PeV-5	20552323		PeV-2	Williamson
PeV-6	21152464		PeV-5	
PeV-5	20552322		PeV-4	K251176
PeV-4	K251176		PeV-2	Williamson

Appendix 6: Viral genome concentrations (copies/µL) of Parechovirus (PeV) isolates determined by RT-qPCR

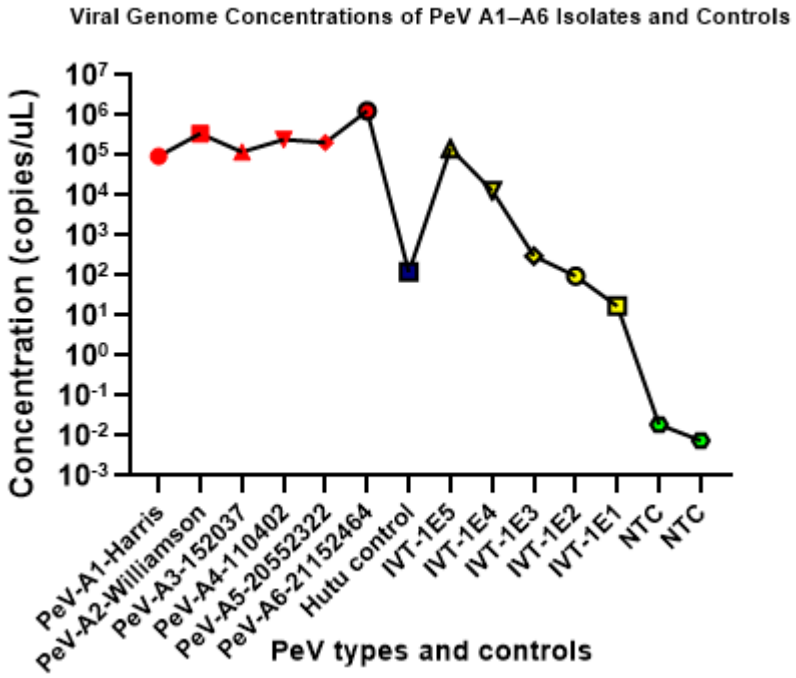

Appendix 7: RT-qPCR result of PeV-A-infected HuTu80 cells with controls and IVT copy numbers

PeV-A Type	Isolate	Ct/Cq	Efficiency R^2	Concentration (Copies/µL)
PeV-A1	Harris	19,47	0,95	9,518E+04
PeV-A1	150-8	20,54	0,94	4,473E+04
PeV-A1	145-12	15,10	0,87	2,172E+06
PeV-A1	103-2	18,04	0,94	2,596E+05
PeV-A2	Williamson	17,62	0,96	3,506E+05
PeV-A2	Williamson	18,25	0,94	2,242E+05
PeV-A2	Williamson	18,14	0,94	2,434E+05
PeV-A3	152037	19,12	0,95	1,223E+05
PeV-A3	K251181-02	27,68	0,88	295,4
PeV-A3	A308/99	17,03	0,99	5,299E+05
PeV-A3	K251181-02	19,39	0,86	1,006E+05
PeV-A3	K251181-02	29,09	0,82	109,4
PeV-A4	110402	18,12	0,94	2,465E+05

PeV-A4	20152401	22,17	0,94	1,424E+04
PeV-A4	K251176	18,65	0,98	1,696E+05
PeV-A4	K251176	17,54	0,97	3,703E+05
PeV-A5	20552323	18,37	0,94	2,064E+05
PeV-A5	20552322	18,34	0,93	2,105E+05
PeV-A5		18,14	0,90	2,428E+05
PeV-A6	21152464	15,75	0,97	1,301E+06
Controls	**Used concentration**	**Ct/Cq**	**Efficiency R²**	**Concentration (Copies/μL)**
Hutu control 1		29,54	0,90	79,72
Hutu control 2		28,94	0,85	122,2
Standard	1E+05	18,84	0,94	1,486E+05
Standard	1E+04	22,29	0,90	1,315E+04
Standard	1E+03	27,64	0,96	305,2
Standard	1E+02	29,27	0,91	96,77
Standard	1E+01	31.72	0,92	17,32
NTC		41,39	0,93	0,01918
NTC		42,72	0,95	0,007545